NUCLEAR SCIENCE COMMITTEE

3-D RADIATION TRANSPORT BENCHMARK PROBLEMS AND RESULTS FOR SIMPLE GEOMETRIES WITH VOID REGIONS

Keisuke Kobayashi
Naoki Sugimura
Yasunobu Nagaya

November 2000

NUCLEAR ENERGY AGENCY
ORGANISATION FOR ECONOMIC CO-OPERATION AND DEVELOPMENT

ORGANISATION FOR ECONOMIC CO-OPERATION AND DEVELOPMENT

Pursuant to Article 1 of the Convention signed in Paris on 14th December 1960, and which came into force on 30th September 1961, the Organisation for Economic Co-operation and Development (OECD) shall promote policies designed:

– to achieve the highest sustainable economic growth and employment and a rising standard of living in Member countries, while maintaining financial stability, and thus to contribute to the development of the world economy;
– to contribute to sound economic expansion in Member as well as non-member countries in the process of economic development; and
– to contribute to the expansion of world trade on a multilateral, non-discriminatory basis in accordance with international obligations.

The original Member countries of the OECD are Austria, Belgium, Canada, Denmark, France, Germany, Greece, Iceland, Ireland, Italy, Luxembourg, the Netherlands, Norway, Portugal, Spain, Sweden, Switzerland, Turkey, the United Kingdom and the United States. The following countries became Members subsequently through accession at the dates indicated hereafter: Japan (28th April 1964), Finland (28th January 1969), Australia (7th June 1971), New Zealand (29th May 1973), Mexico (18th May 1994), the Czech Republic (21st December 1995), Hungary (7th May 1996), Poland (22nd November 1996) and the Republic of Korea (12th December 1996). The Commission of the European Communities takes part in the work of the OECD (Article 13 of the OECD Convention).

NUCLEAR ENERGY AGENCY

The OECD Nuclear Energy Agency (NEA) was established on 1st February 1958 under the name of the OEEC European Nuclear Energy Agency. It received its present designation on 20th April 1972, when Japan became its first non-European full Member. NEA membership today consists of 27 OECD Member countries: Australia, Austria, Belgium, Canada, Czech Republic, Denmark, Finland, France, Germany, Greece, Hungary, Iceland, Ireland, Italy, Japan, Luxembourg, Mexico, the Netherlands, Norway, Portugal, Republic of Korea, Spain, Sweden, Switzerland, Turkey, the United Kingdom and the United States. The Commission of the European Communities also takes part in the work of the Agency.

The mission of the NEA is:

– to assist its Member countries in maintaining and further developing, through international co-operation, the scientific, technological and legal bases required for a safe, environmentally friendly and economical use of nuclear energy for peaceful purposes, as well as
– to provide authoritative assessments and to forge common understandings on key issues, as input to government decisions on nuclear energy policy and to broader OECD policy analyses in areas such as energy and sustainable development.

Specific areas of competence of the NEA include safety and regulation of nuclear activities, radioactive waste management, radiological protection, nuclear science, economic and technical analyses of the nuclear fuel cycle, nuclear law and liability, and public information. The NEA Data Bank provides nuclear data and computer program services for participating countries.

In these and related tasks, the NEA works in close collaboration with the International Atomic Energy Agency in Vienna, with which it has a Co-operation Agreement, as well as with other international organisations in the nuclear field.

FOREWORD

Several NEA Nuclear Science Committee (NSC) activities are concerned with the validation of computation methods and codes as applied to nuclear technology. One of the challenges has been and continues to be the refined modelling of the full geometrical complexity of real problems in practical applications. Two types of method for three-dimensional modelling have emerged: the stochastic Monte Carlo method and several deterministic methods.

In order to address current issues in this field, a series of 3-D neutron transport benchmarks, known as "Takeda benchmarks" were organised under the auspices of the NSC (Report NEACRP-L-330, March 1991), and concerned small, highly heterogeneous reactor cores. The Workshop on Advanced Monte Carlo Computer Programs for Radiation Transport was then organised in Saclay, France on 27-29 April 1993 (proceedings published in 1995 as ISBN 92-64-14376-9), followed by a seminar entitled "3-D Deterministic Radiation Transport Computer Programs: Features, Applications and Perspectives", which was held in Paris on 2-3 December 1996 (proceedings published in 1997 as ISBN 92-64-16020-5).

One of the results of the latter seminar was the decision to organise an additional benchmark study so as to clarify issues of precision regarding the different methods used for flux calculations. A proposal was made by Professor Keisuke Kobayashi from the University of Kyoto to study a pure absorber problem with internal void regions, which was then further extended to include cases with 50% scattering. This set of problems is known as the "Kobayashi benchmarks".

The results of these benchmarks were discussed at a meeting in Madrid, Spain on 1 October 1999, hosted by the Consejo de Energía Nuclear. The re-analysis of the results presented then are summarised in this report and compared with the "exact" reference solutions.

The participants have agreed to publish the results of each of the codes used along with separate, detailed discussion papers in a special issue of *Progress in Nuclear Energy* in 2001.

Further needs for validating methods have been identified and a new benchmark was recently launched recently by the NSC. It concerns a pin-by-pin power distribution within core assemblies using transport theory in seven energy groups. This is particularly relevant when validating the computation of anisotropy effects in highly heterogeneous systems. Professor Elmer Lewis from Northwestern University and members of Argonne National Laboratory have prepared the specification for this benchmark. The results will be published in a future report.

Acknowledgements

International benchmark studies require the dedicated participation and contribution of the best experts available. We wish to acknowledge the valuable contribution of all participants and express our thanks for their efforts to make this project successful. The authors would like to recognise the contribution of Richard Sanchez for providing exact values of the pure absorber cases, Enrico Sartori of the NEA for his support of this benchmark, and Edgar Kiefhaber of Forschungszentrum Karlsruhe and Yousry Azmy of Oak Ridge National Laboratory for their useful comments on the manuscript.

Particular thanks go to Professor Emeritus Keisuke Kobayashi, who designed the benchmark and co-ordinated its related activities, and to Masayuki Nakagawa and Luis Garcia de Viedma for representing the NSC and providing helpful support. Finally, thanks go to Amanda Costa who was responsible for the final editing of the report.

TABLE OF CONTENTS

Introduction

In the OECD proceedings on 3-D deterministic radiation transport computer programs edited by E. Sartori [1], many 3-D deterministic transport programs were presented. It is not simple, however, to determine their special features or their accuracy. One of the difficulties in multi-dimensional transport calculations concerns the accuracy of the flux distribution for systems which have void regions in a highly absorbing medium.

The method most widely used to solve the 3-D transport equation is the discrete ordinates method. However, this method has the disadvantage of the ray effect and we must be cautious which S_n order and which quadrature set for the angular discretisation should be used for such systems. On the other hand, the spherical harmonics method has the advantage of causing no ray effect, but the equations are very complicated and it is difficult to derive the finite difference or discrete equations which satisfy the necessary boundary conditions at material interfaces as discussed by Kobayashi [2]. Then, the flux distribution by the spherical harmonics method shows some anomalies at the material interfaces of large cross-section differences or at the material void interface. This was seen in the flux distribution of the 3-D benchmark calculations with void region proposed by Takeda [3], in which appreciable discrepancies were observed in the flux distribution between programs based on the spherical harmonics method as shown by Kobayashi [2].

Ackroyd and Riyait [4] investigated flux distributions for 2-D void problems extensively, and their results show that these void problems are really difficult, suggesting that 3-D transport programs should also be checked for these problems.

The 3-D benchmark void problems of simple geometries proposed at the OECD/NEA in 1996 by Kobayashi [5] which were simple extensions of the 2-D void problems given by Ackroyd and Riyait to 3-D geometries. There are two kinds of one-group source problems. One is a system of a pure absorber with a void region so that the exact solution can be obtained by numerical integration. The other one has the same geometry as the pure absorber problem, however, the pure absorber is replaced by a material which has a scattering cross-section of 50% of the total cross-section intended as the case where ray effects are not too large. Preliminary results were presented at the Madrid conference by Kobayashi, *et al*. [6].

Benchmark problems

The systems consist of three regions, source, void and shield regions, whose geometries are shown in Figures 1-8. An $x - z$ or $y - z$ plane geometry and a sketch of Problem 1 are shown in Figures 1 and 2, respectively. An $x - y$ or $y - z$ plane geometry and a sketch of Problem 2 are shown in Figures 3 and 4, respectively. Plane geometries and a sketch of Problem 3 are shown in Figures 5-8, which is called the dog leg void duct problem. Reflective boundary conditions are used at the boundary planes $x = 0$, $y = 0$ and $z = 0$, and vacuum boundary conditions at all outer boundaries for all problems.

The cross-sections and source strength S are shown in Table 1. The cross-section in a void region is assumed to be not zero but 10^{-4} cm^{-1} so that 3-D transport programs based on the second order differential form can be used.

In Problems 1-i, 2-i and 3-i, the systems consist of a pure absorber, and in Problems 1-ii, 2-ii and 3-ii, the systems have a scattering cross-section of 50% of the total cross-section, namely, $\Sigma_s = 0.5\Sigma_t$. It is expected that the total flux distributions at mesh points shown in Tables 2-4 be calculated. These mesh points are chosen so that the programs which give the fluxes at the mesh centre can be used. The mesh width, CPU time, the required memory size and the name of the computer used should be given.

Problem 1

Figure 1. $x-z$ or $y-z$ plane of Problem 1, shield with square void

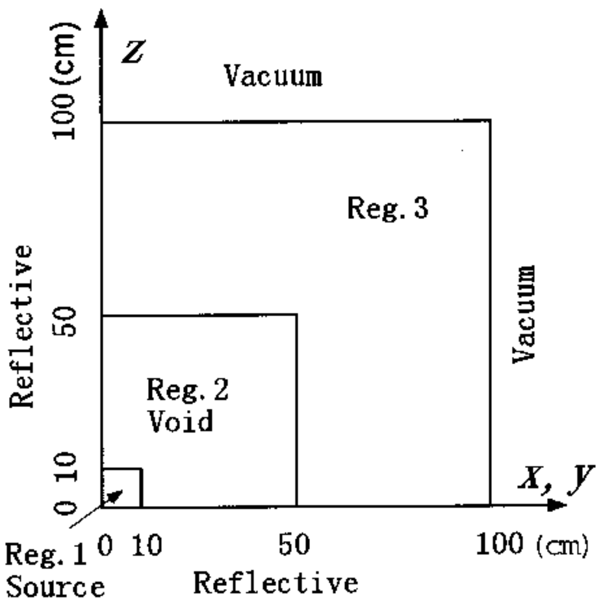

Figure 2. Sketch of Problem 1, shield with square void

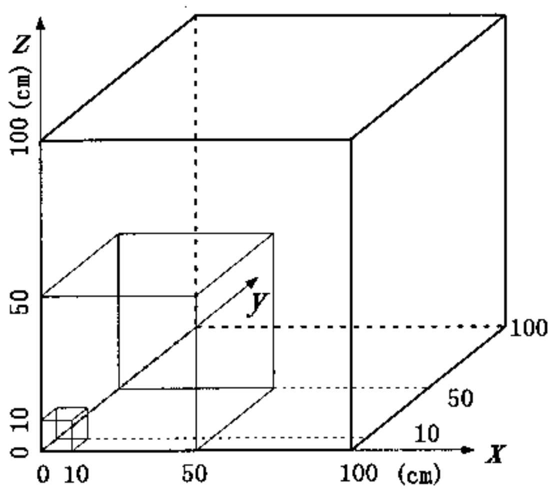

Problem 2

Figure 3. $x-y$ or $y-z$ plane of Problem 2, shield with void duct

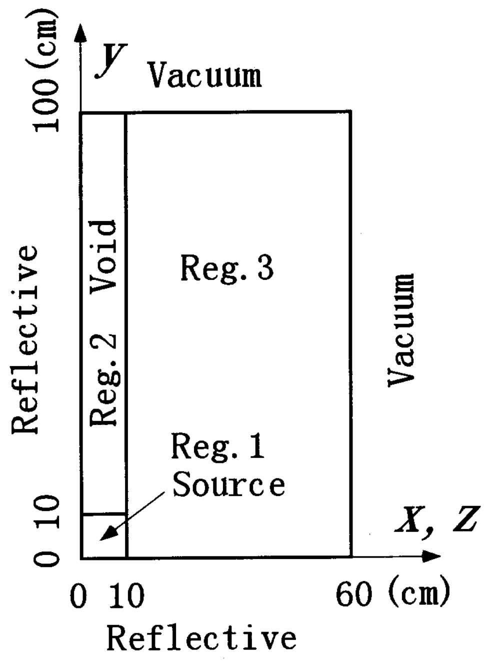

Figure 4. Sketch of Problem 2, shield with void duct

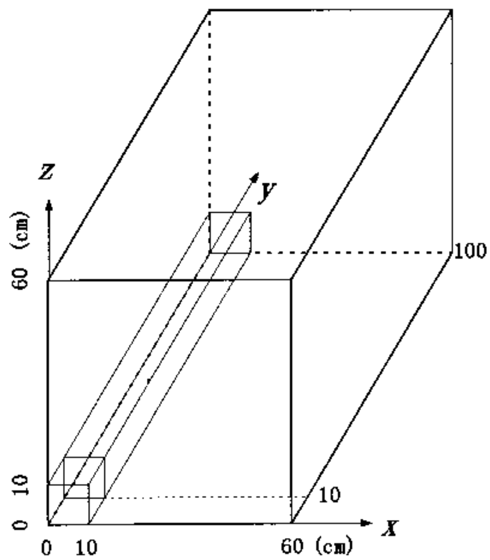

Problem 3

Figure 5. ***x – y*** **plane of Problem 3, shield with dog leg void duct**

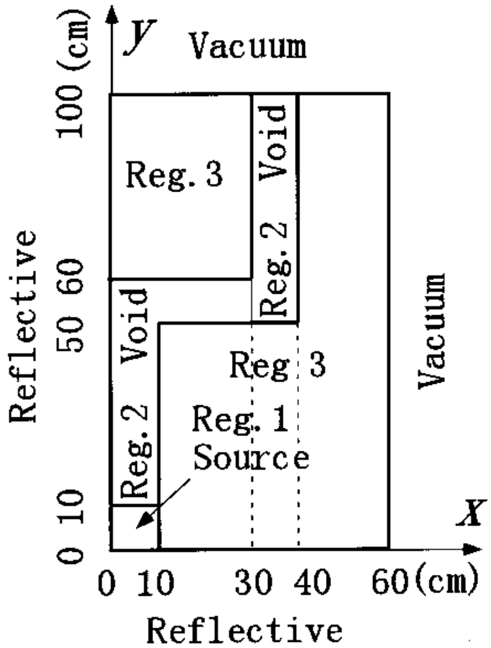

Figure 6. ***y – z*** **plane of Problem 3, shield with dog leg void duct**

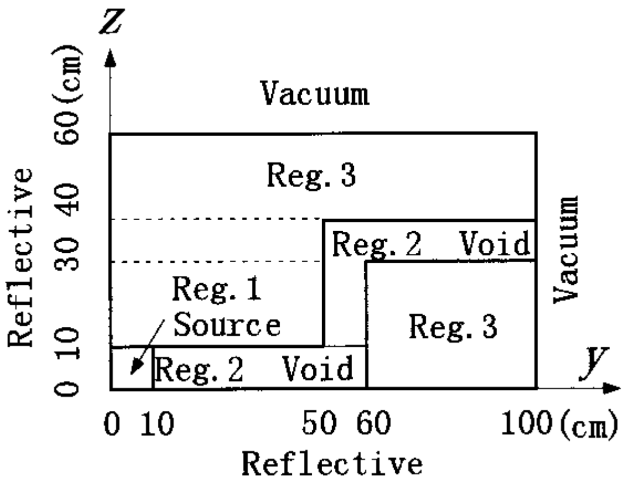

Figure 7. $x - z$ plane of Problem 3, shield with dog leg void duct

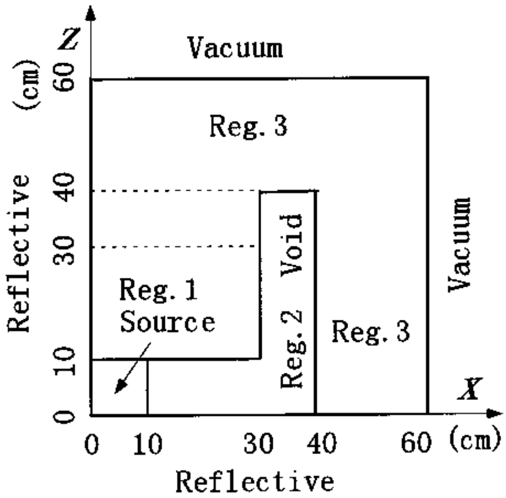

Figure 8. Sketch of Problem 3, shield with dog leg void duct

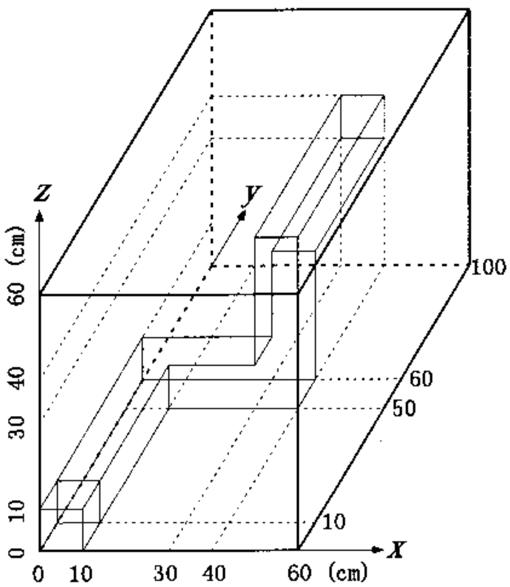

Table 1. One-group cross-sections and source strength *S*

Region	S (n cm^{-3}s^{-1})	Σ_t (cm^{-1})	Problem i Σ_s (cm^{-1})	Problem ii Σ_s (cm^{-1})
1	1	0.1	0	0.05
2	0	10^{-4}	0	0.5×10^{-4}
3	0	0.1	0	0.05

Reference solutions

Exact total flux for pure absorber problems

In the case of no scattering, fluxes can be obtained simply by numerical integration; namely, the neutron total flux at the observation position $\boldsymbol{r}$ in a pure absorber can be calculated by:

$$\phi(\boldsymbol{r}) = \frac{1}{4\pi}\int_{V_s} d\boldsymbol{r}' \frac{\exp\left(-\int \Sigma_a(\boldsymbol{r}'')d\boldsymbol{r}''\right)S(\boldsymbol{r}')}{\left|\boldsymbol{r}-\boldsymbol{r}'\right|^2} \tag{1}$$

where $\phi(\boldsymbol{r})$, $S(\boldsymbol{r}')$, Σ_a and V_s are the total flux, external source, absorption cross-section and source region, respectively.

We assume that the source $S(\boldsymbol{r})$ is constant in space and use the relation:

$$\boldsymbol{l} = \boldsymbol{r}' - \boldsymbol{r}, \qquad d,\boldsymbol{r}' = d\boldsymbol{l} = l^2 dl d\Omega = l^2 dl \sin\theta d\varphi d\theta \tag{2}$$

where θ and φ are the polar and azimuthal angles, respectively.

If the observation position $\boldsymbol{r}$ is at the outside of the source region as shown in Figure 9, the total flux of Eq. (1) can be expressed as:

$$\begin{aligned}\phi(\boldsymbol{r}) &= \frac{1}{4\pi}\int_{V_s} d\boldsymbol{l} \frac{\exp\left(-\int_0^{l_a}\Sigma_a(\boldsymbol{l}')dl' - \int_{l_a}^{l}\Sigma_a(\boldsymbol{l}')dl'\right)S(\boldsymbol{l})}{l^2} \\ &= \frac{S}{4\pi}\int d\Omega \int_{l_a}^{l_b} l^2 dl \frac{\exp(-\Sigma_{a1}l_1 - \Sigma_{a0}l_0)\exp\left(-\int_{l_a}^{l}\Sigma_{a1}dl'\right)}{l^2} \\ &= \frac{S}{4\pi\Sigma_{a1}}\int d\Omega \exp(-\Sigma_{a1}l_1 - \Sigma_{a0}l_0)\left(1-\exp\left(-\Sigma_{a1}(l_b - l_a)\right)\right)\end{aligned} \tag{3}$$

where the external source is assumed to be in the region whose absorption cross-section is Σ_{a1}, l_0 and l_1 are the total length of the path whose absorption cross-sections are Σ_{a0} and Σ_{a1}, respectively, and l_b - l_a is the path length in the source region. If the observation position $\boldsymbol{r}$ is in the inside of the source region as shown in Figure 10, the total flux of Eq. (1) becomes:

$$\begin{aligned}\phi(\boldsymbol{r}) &= \frac{1}{4\pi}\int_{V_s} d\boldsymbol{l} \frac{\exp\left(-\int_0^{l}\Sigma_a(\boldsymbol{l}')dl'\right)S(\boldsymbol{l})}{l^2} = \frac{S}{4\pi}\int d\Omega \int_0^{l_b} l^2 dl \frac{\exp(-\Sigma_{a1}l)}{l^2} \\ &= \frac{S}{4\pi\Sigma_{a1}}\int d\Omega\left(1-\exp(-\Sigma_{a1}l_b)\right)\end{aligned} \tag{4}$$

where l_b is the length of the path from the observation position $\boldsymbol{r}$ to the boundary of the source region.

The total fluxes given by Eqs. (3) and (4) are calculated using the trapezoidal rule in θ and φ variables, where the number of mesh points used for both θ and φ variables is 20 000. Convergence with respect to the number of mesh points is checked by comparing the fluxes with 10 000 mesh points and confirming that there is no difference between them. The fluxes thus obtained are shown in Tables 2, 3 and 4 for each problem.

Figure 9. Observation point is outside the source region

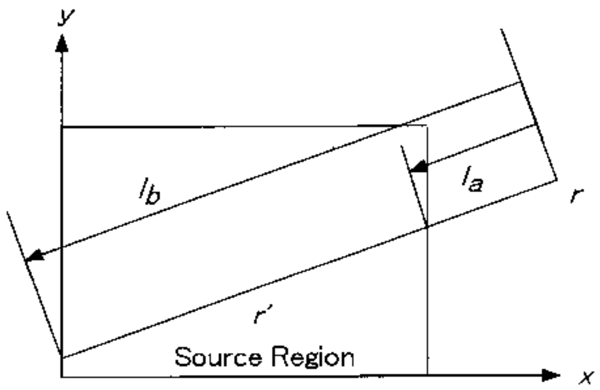

Figure 10. Observation point is inside the source region

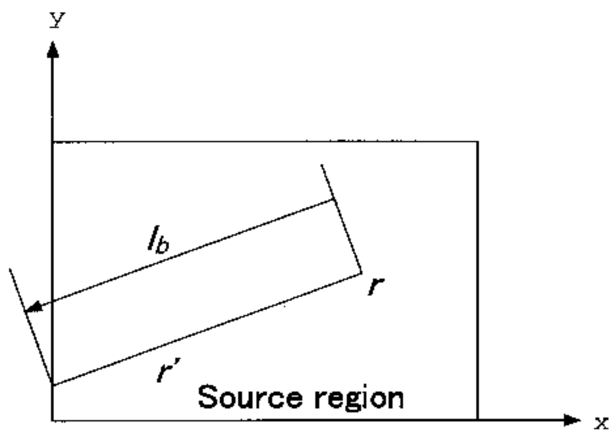

Table 2. Total flux for Problem 1

Case	Co-ordinates	Case i (no scattering)			Case ii (50% scattering)	
		Analytical method	Monte Carlo method by GMVP			
	(cm) (x,y,z)	Total flux $(cm^{-2}s^{-1})$	Total flux $(cm^{-2}s^{-1})$	FSD[a] $1\sigma(\%)$	Total flux $(cm^{-2}s^{-1})$	FSD $1\sigma(\%)$
1A	5, 5, 5	5.95659×10^{-0}	5.95332×10^{-0}	0.308	8.29260×10^{-0}	0.021
	5, 15, 5	1.37185×10^{-0}	1.37116×10^{-0}	0.053	1.87028×10^{-0}	0.005
	5, 25, 5	5.00871×10^{-1}	5.00789×10^{-1}	0.032	7.13986×10^{-1}	0.003
	5, 35, 5	2.52429×10^{-1}	2.52407×10^{-1}	0.027	3.84685×10^{-1}	0.004
	5, 45, 5	1.50260×10^{-1}	1.50251×10^{-1}	0.025	2.53984×10^{-1}	0.006
	5, 55, 5	5.95286×10^{-2}	5.95254×10^{-2}	0.023	1.37220×10^{-1}	0.073
	5, 65, 5	1.53283×10^{-2}	1.53274×10^{-2}	0.022	4.65913×10^{-2}	0.117
	5, 75, 5	4.17689×10^{-3}	4.17666×10^{-3}	0.022	1.58766×10^{-2}	0.197
	5, 85, 5	1.18533×10^{-3}	1.18527×10^{-3}	0.021	5.47036×10^{-3}	0.343
	5, 95, 5	3.46846×10^{-4}	3.46829×10^{-4}	0.021	1.85082×10^{-3}	0.619

[a] Fractional standard deviation

Table 2. Total flux for Problem 1 (*cont.*)

Case	Co-ordinates (cm) (*x*,*y*,*z*)	Case i (no scattering) Analytical method Total flux ($cm^{-2}s^{-1}$)	Case i (no scattering) Monte Carlo method by GMVP Total flux ($cm^{-2}s^{-1}$)	FSD[a] 1σ(%)	Case ii (50% scattering) Monte Carlo method by GMVP Total flux ($cm^{-2}s^{-1}$)	FSD 1σ(%)
1B	5, 5, 5	5.95659×10^{-0}	5.95332×10^{-0}	0.308	8.29260×10^{-0}	0.021
	15, 15, 15	4.70754×10^{-1}	4.70489×10^{-1}	0.040	6.63233×10^{-1}	0.004
	25, 25, 25	1.69968×10^{-1}	1.69911×10^{-1}	0.025	2.68828×10^{-1}	0.003
	35, 35, 35	8.68334×10^{-2}	8.68104×10^{-2}	0.021	1.56683×10^{-1}	0.005
	45, 45, 45	5.25132×10^{-2}	5.25011×10^{-2}	0.020	1.04405×10^{-1}	0.011
	55, 55, 55	1.33378×10^{-2}	1.33346×10^{-2}	0.019	3.02145×10^{-2}	0.061
	65, 65, 65	1.45867×10^{-3}	1.45829×10^{-3}	0.019	4.06555×10^{-3}	0.074
	75, 75, 75	1.75364×10^{-4}	1.75316×10^{-4}	0.019	5.86124×10^{-4}	0.116
	85, 85, 85	2.24607×10^{-5}	2.24543×10^{-5}	0.019	8.66059×10^{-5}	0.198
	95, 95, 95	3.01032×10^{-6}	3.00945×10^{-6}	0.019	1.12892×10^{-5}	0.383
1C	5, 55, 5	5.95286×10^{-2}	5.95254×10^{-2}	0.023	1.37220×10^{-1}	0.073
	15, 55, 5	5.50247×10^{-2}	5.50191×10^{-2}	0.023	1.27890×10^{-1}	0.076
	25, 55, 5	4.80754×10^{-2}	4.80669×10^{-2}	0.022	1.13582×10^{-1}	0.080
	35, 55, 5	3.96765×10^{-2}	3.96686×10^{-2}	0.021	9.59578×10^{-2}	0.088
	45, 55, 5	3.16366×10^{-2}	3.16291×10^{-2}	0.021	7.82701×10^{-2}	0.094
	55, 55, 5	2.35303×10^{-2}	2.35249×10^{-2}	0.020	5.67030×10^{-2}	0.111
	65, 55, 5	5.83721×10^{-3}	5.83626×10^{-3}	0.020	1.88631×10^{-2}	0.189
	75, 55, 5	1.56731×10^{-3}	1.56708×10^{-3}	0.020	6.46624×10^{-3}	0.314
	85, 55, 5	4.53113×10^{-4}	4.53048×10^{-4}	0.020	2.28099×10^{-3}	0.529
	95, 55, 5	1.37079×10^{-4}	1.37060×10^{-4}	0.020	7.93924×10^{-4}	0.890

[a] Fractional standard deviation

Table 3. Total flux for Problem 2

Case	Co-ordinates (cm) (*x*,*y*,*z*)	Case i (no scattering) Analytical method Total flux ($cm^{-2}s^{-1}$)	Case i (no scattering) Monte Carlo method by GMVP Total flux ($cm^{-2}s^{-1}$)	FSD[a] 1σ(%)	Case ii (50% scattering) Monte Carlo method by GMVP Total flux ($cm^{-2}s^{-1}$)	FSD 1σ(%)
2A	5, 5, 5	5.95659×10^{-0}	5.94806×10^{-0}	0.287	8.61696×10^{-0}	0.063
	5, 15, 5	1.37185×10^{-0}	1.37199×10^{-0}	0.055	2.16123×10^{-0}	0.015
	5, 25, 5	5.00871×10^{-1}	5.00853×10^{-1}	0.034	8.93437×10^{-1}	0.011
	5, 35, 5	2.52429×10^{-1}	2.52419×10^{-1}	0.029	4.77452×10^{-1}	0.012
	5, 45, 5	1.50260×10^{-1}	1.50256×10^{-1}	0.027	2.88719×10^{-1}	0.013
	5, 55, 5	9.91726×10^{-2}	9.91698×10^{-2}	0.025	1.88959×10^{-1}	0.014
	5, 65, 5	7.01791×10^{-2}	7.01774×10^{-2}	0.024	1.31026×10^{-1}	0.016
	5, 75, 5	5.22062×10^{-2}	5.22050×10^{-2}	0.023	9.49890×10^{-2}	0.017
	5, 85, 5	4.03188×10^{-2}	4.03179×10^{-2}	0.023	7.12403×10^{-2}	0.019
	5, 95, 5	3.20574×10^{-2}	3.20568×10^{-2}	0.022	5.44807×10^{-2}	0.019

[a] Fractional standard deviation

Table 3. Total flux for Problem 2 (*cont.*)

Case	Co-ordinates	Case i (no scattering)			Case ii (50% scattering)	
		Analytical method	Monte Carlo method by GMVP			
	(cm) (x,y,z)	Total flux $(cm^{-2}s^{-1})$	Total flux $(cm^{-2}s^{-1})$	FSD[a] $1\sigma(\%)$	Total flux $(cm^{-2}s^{-1})$	FSD $1\sigma(\%)$
2B	5, 95, 5	3.20574×10^{-2}	3.20568×10^{-2}	0.022	5.44807×10^{-2}	0.019
	15, 95, 5	1.70541×10^{-3}	1.70547×10^{-3}	0.040	6.58233×10^{-3}	0.244
	25, 95, 5	1.40557×10^{-4}	1.40555×10^{-4}	0.046	1.28002×10^{-3}	0.336
	35, 95, 5	3.27058×10^{-5}	3.27057×10^{-5}	0.044	4.13414×10^{-4}	0.363
	45, 95, 5	1.08505×10^{-5}	1.08505×10^{-5}	0.042	1.55548×10^{-4}	0.454
	55, 95, 5	4.14132×10^{-6}	4.14131×10^{-6}	0.039	6.02771×10^{-5}	0.599

[a] Fractional standard deviation

Table 4. Total flux for Problem 3

Case	Co-ordinates	Case i (no scattering)			Case ii (50% scattering)	
		Analytical method	Monte Carlo method by GMVP			
	(cm) (x,y,z)	Total flux $(cm^{-2}s^{-1})$	Total flux $(cm^{-2}s^{-1})$	FSD[a] $1\sigma(\%)$	Total flux $(cm^{-2}s^{-1})$	FSD $1\sigma(\%)$
3A	5, 5, 5	5.95659×10^{-0}	5.93798×10^{-0}	0.306	8.61578×10^{-0}	0.044
	5, 15, 5	1.37185×10^{-0}	1.37272×10^{-0}	0.052	2.16130×10^{-0}	0.010
	5, 25, 5	5.00871×10^{-1}	5.01097×10^{-1}	0.032	8.93784×10^{-1}	0.008
	5, 35, 5	2.52429×10^{-1}	2.52517×10^{-1}	0.027	4.78052×10^{-1}	0.008
	5, 45, 5	1.50260×10^{-1}	1.50305×10^{-1}	0.025	2.89424×10^{-1}	0.009
	5, 55, 5	9.91726×10^{-2}	9.91991×10^{-2}	0.024	1.92698×10^{-1}	0.010
	5, 65, 5	4.22623×10^{-2}	4.22728×10^{-2}	0.023	1.04982×10^{-1}	0.077
	5, 75, 5	1.14703×10^{-2}	1.14730×10^{-2}	0.022	3.37544×10^{-2}	0.107
	5, 85, 5	3.24662×10^{-3}	3.24736×10^{-3}	0.021	1.08158×10^{-2}	0.163
	5, 95, 5	9.48324×10^{-4}	9.48534×10^{-4}	0.021	3.39632×10^{-3}	0.275
3B	5, 55, 5	9.91726×10^{-2}	9.91991×10^{-2}	0.024	1.92698×10^{-1}	0.010
	15, 55, 5	2.45041×10^{-2}	2.45184×10^{-2}	0.035	6.72147×10^{-2}	0.019
	25, 55, 5	4.54477×10^{-3}	4.54737×10^{-3}	0.037	2.21799×10^{-2}	0.028
	35, 55, 5	1.42960×10^{-3}	1.43035×10^{-3}	0.034	9.90646×10^{-3}	0.033
	45, 55, 5	2.64846×10^{-4}	2.64959×10^{-4}	0.032	3.39066×10^{-3}	0.195
	55, 55, 5	9.14210×10^{-5}	9.14525×10^{-5}	0.029	1.05629×10^{-3}	0.327
3C	5, 95, 35	3.27058×10^{-5}	3.27087×10^{-5}	0.045	3.44804×10^{-4}	0.793
	15, 95, 35	2.68415×10^{-5}	2.68518×10^{-5}	0.047	2.91825×10^{-4}	0.659
	25, 95, 35	1.70019×10^{-5}	1.70104×10^{-5}	0.047	2.05793×10^{-4}	0.529
	35, 95, 35	3.37981×10^{-5}	3.38219×10^{-5}	0.043	2.62086×10^{-4}	0.075
	45, 95, 35	6.04893×10^{-6}	6.05329×10^{-6}	0.042	1.05367×10^{-4}	0.402
	55, 95, 35	3.36460×10^{-6}	3.36587×10^{-6}	0.028	4.44962×10^{-5}	0.440

[a] Fractional standard deviation

Suslov, *et al*. [7] also calculated the fluxes from Eq. (1) using three-dimensional numerical quadrature, and their fluxes are exactly the same as the present ones for all six digits given in Tables 2, 3 and 4 except small differences at mesh points (45,95,35) and (55,95,35) of Problem 3.

Monte Carlo results by GMVP

Monte Carlo calculations were also performed using GMVP [8], where a point-detector estimator was used to tally the total flux at the given calculation points for all cases. In the pure absorber cases, 10^7 histories were used, and for the 50% scattering cases, 10^9, 10^8 and 2×10^8 histories for Problems 1, 2 and 3, respectively. Calculated total fluxes are shown in Tables 2-4. The total fluxes for the pure absorber cases are in very good agreement with the analytical results, which shows that the GMVP program is reliable for these kind of problems. Konno [9] also calculated the total flux using MCNP4B2, and his results agree well with the present results within statistical errors.

Benchmark results

As shown in Table 5, there are eight contributions for the present benchmarks. Six contributions were obtained by using discrete ordinates method programs. They are: TORT by Azmy, *et al*. at ORNL [10], TORT with FNSUNCL3 by Konno at JAERI [9,11], PARTISN by Alcouffe at LANL [12], PENTRAN by Haghighat and Sjoden at PSU and USAF respectively [13], IDT by Zmijarevic at CEA [14] and MCCG3D by Suslov, *et al*. at IPPE, UTK and CEA [7]. The other two contributions were obtained using the spherical harmonics method, EVENT by Oliveira, *et al*. at IC [15], and ARDRA by Brown, *et al*. at LLNL [16].

Table 5. 3-D transport benchmark results

Name	Program	Method	Problems	Mesh width (cm)	Computer
Azmy, *et al*.	TORT	S_{16} LN[a]	Scattering cases only	10/9	Cray Y/MP 4 tasks
Konno	TORT TORT with FNSUNCL3	S_{16} S_{16} FCS[b]	All cases All cases	2 2 0.25	FUJITSU AP3000/24
Alcouffe	PARTISN	S_8, FC[b]	All cases	2	SGI
Haghighat, *et al*.	PENTRAN	S_{20}, ADS[c] S_{12}, ADS[c]	No scattering Scattering	Variable (2-10) 1.111	IBM SP2 IBM SP2
Zmijarevic	IDT	S_{16}, LC[d] Extrapolated	All cases	(10/9)	DEC Alpha 4100
Suslov, *et al*.	MCCG3D	RT[e], SC[f], DD[g]	All cases	2.5	SP2
Oliveira, *et al*.	EVENT	P_9, RT[e]	All cases	1.43-2	COMPAQ AXP 1000
Brown, *et al*.	ARDRA	P_{21}	All cases	1.04-2	IBM ASCI Blue-Pacific

[a] Linear nodal, [b] First collision source, [c] Adaptive differencing strategy using the DTW and EDW schemes,
[d] Linear characteristic, [e] Ray tracing, [f] Step characteristic, [g] Diamond difference

In the results by Konno, there are two cases, one in which only TORT is used, and the other in which TORT is used together with the program FNSUNCL3 and for which the first flight collision source is calculated. In the finite element-spherical harmonics solutions by EVENT, the ray-tracing method has been used in the void region, and the flux values are quoted only for points within the domain of the non-void region, since fluxes in the ray-tracing regions were not available with the current implementation.

Benchmark results for Problem (i) of no scattering and (ii) of 50% scattering for Problems 1, 2 and 3 are shown in Figures 11-42. Shown in these figures are the scattering cases calculated with TORT by Azmy, and the no-scattering cases calculated with TORT by Konno. In Figures 12, 14, etc., the ratios of the fluxes to the reference values (i.e. the exact values by the analytical method for the pure absorber cases, and the Monte Carlo values for the scattering cases) are shown in order to make clear the difference from the reference values.

Discussion and conclusion

The benchmark results shown in Figures 11-42 are fairly close to the reference solutions, although some preliminary results have discrepancies with regard to the reference solutions. In the case of the pure absorber, the apparent discrepancies of the discrete ordinates program TORT (JAERI) from the exact values for problems 1Ci, 2Bi and 3Ci may be due to the ray effect. Namely, even the S_{16} method gives appreciable errors due to ray effects.

In the cases with 50% scattering, the total fluxes for the problems, for example, 1Cii, 2Bii and 3Cii are larger by about a factor of 10 than those for pure absorber cases of 1Ci, 2Bi and 3Ci, respectively. Namely, the number of scattered neutrons is larger by about a factor of 10 than the neutrons which come directly from the source, and the ray effect becomes smaller even in TORT. However, discrepancies from the exact values are fairly large for the problem of the dog leg duct, problems 3Ci and 3Cii. In the discrete ordinates programs TORT, PENTRAN and IDT, the first collision source was not used. In PENTRAN, the ray effect is remedied by using appropriate angular and spatial meshes and mesh widths, and PENTRAN's unique differencing formulations including adaptive differencing strategy with directional theta-weighted (DTW) and exponential directional weighted (EDW) schemes and Taylor projection mesh coupling (TPMC) [13].

In other discrete ordinates programs, TORT with FNSUNCL3, PARTISN and MCCG3D, the first collision source was used to remedy the ray effect, which is seen in figures given by Konno [9] to be very successful. Namely, the use of the first collision source for the discrete ordinates method appreciably improved the accuracy for both problems of pure absorber and 50% scattering cases. In particular, the results of MCCG3D and TORT with FNSUNCL3 are in excellent agreement, within an error of 1-5% with the reference solution in most cases, and can be considered as an independent confirmation of the reference solution. It should be noted that, for the pure absorber problems, the first collision source method should give in principle exact fluxes and this fact does not demonstrate the accuracy of the discrete ordinate method itself.

An advantage of the spherical harmonics method is that the equations are invariant under rotation of the co-ordinates and do not depend on the direction of the co-ordinates that should give no ray effect. In order to overcome the difficulty in deriving the discretised equations of the spherical harmonics method for void problems, the ray-tracing method was used for the void region in the spherical harmonics program EVENT, and the flux in non-void region was coupled with the current in the void region at the void-material interface. Using this method, the accuracy of the current spherical harmonics method program was improved. In the program ARDRA, the discrete ordinates equations with a fictitious source were solved in such a way that the equations became equivalent to those of the spherical harmonics method, which were used to solve two-dimensional spherical harmonics equations [17,18].

As seen in the figures, the accuracy of the discrete ordinates method with the first collision source is best for the present benchmark problems. It is expected that the present benchmark problem would help further improvement of 3-D transport programs based on the spherical harmonics method as well as the discrete ordinates method.

REFERENCES

[1] "3-D Deterministic Radiation Transport Computer Programs: Features, Applications and Perspectives", E. Sartori, ed., OECD Proceedings, Nuclear Energy Agency (1997).

[2] K. Kobayashi, "On the Advantage of the Finite Fourier Transformation Method for the Solution of a Multi-Group Transport Equation by the Spherical Harmonics Method", *Transp. Theory Statis. Phys.*, 24, 113 (1995).

[3] T. Takeda, H. Ikeda, "3-D Neutron Transport Benchmarks", NEACRP-L-330 (1991).

[4] R.T. Ackroyd, N.S. Riyait, "Iteration and Extrapolation Method for the Approximate Solution of the Even-Parity Transport Equation for Systems with Voids", *Ann. Nucl. Energy*, 16, 1 (1989).

[5] K. Kobayashi, "A Proposal for 3-D Radiation Transport Benchmarks for Simple Geometries with Void Region, 3-D Deterministic Radiation Transport Computer Programs", OECD Proceedings, p. 403 (1997).

[6] K. Kobayashi, N. Sugimura, Y. Nagaya, "3-D Radiation Transport Benchmarks for Simple Geometries with Void Region", M&C '99, Mathematics and Computation, Reactor Physics and Environmental Analysis in Nuclear Applications, Madrid, p. 657 (CD), 27-30 Sept. (1999).

[7] I. Suslov, R. Sanchez and I. Zmijarevic, "Deterministic Reference Solution for 3-D Kobayashi Benchmarks", M&C '99, Mathematics and Computation, Reactor Physics and Environmental Analysis in Nuclear Applications, Madrid, p. 1765 (CD), 27-30 Sept. (1999).

[8] T. Mori and M. Nakagawa, "MVP/GMVP: General Purpose Monte Carlo Codes", JAERI-Data/ Code 94-007 (1994) [in Japanese].

[9] C. Konno, "TORT Solutions with FNSUNCL3 on 3-D Radiation Transport Benchmarks for Simple Geometry with Void Region", M&C '99, Mathematics and Computation, Reactor Physics and Environmental Analysis in Nuclear Applications, Madrid, p. 1755 (CD), 27-30 Sept. (1999).

[10] Y.Y. Azmy, F.X. Gallmeier and R.A. Lillie, "TORT Solutions for the 3-D Radiation Transport Benchmarks for Simple Geometry with Void Region", M&C '99, Mathematics and Computation, Reactor Physics and Environmental Analysis in Nuclear Applications, Madrid, p. 1745 (CD), 27-30 September (1999).

[11] K. Kosako, C. Konno, "FNSUNCL3 – GRTUNCL Code for TORT", JAERI/Review 98-022, p. 140 (1998). See also K. Kosako and C. Konno, "FNSUNCL3: First Collision Source Code for TORT", ICRS-9, Proc. of the Ninth International Conference on Radiation Shielding, Tsukuba, 17-22 October 1999, *Journal of Nuclear Science and Technology,* Supplement 1, March 2000, p. 475 (2000).

[12] R. Alcouffe, to be published in *Progress in Nuclear Energy* (2000).

[13] A. Haghighat, G.E. Sjoden, "Significance of Adaptive Differencing, Variable Grid Density and TPMC for S_n Methods", M&C '99, Mathematics and Computation, Reactor Physics and Environmental Analysis in Nuclear Applications, Madrid, p. 1775 (CD), 27-30 Sept. (1999).

[14] I. Zmijarevic, to be published in *Progress in Nuclear Energy* (2000).

[15] C.R.E. Oliveira, *et al.*, private communication (1999).

[16] P.N. Brown, B. Chang and U.R. Hanebutte, "Spherical Harmonic Solutions to the 3-D Kobayashi Benchmark Suite", Proceedings of the PHYSOR 2000, ANS International Topical Meeting on Advances in Reactor Physics and Mathematics and Computation into the Next Millennium, 7-12 May 2000, Pittsburgh, Pennsylvania, USA (2000).

[17] WM.H. Reed, "Spherical Harmonics Solutions of the Neutron Transport Equation from Discrete Ordinate Codes", *Nucl. Sci. Eng.*, 49, 10 (1972).

[18] J. Jung, *et al.*, "Numerical Solutions of Discrete-Ordinate Neutron Transport Equations Equivalent to P_L Approximation in $X - Y$ Geometry", *J. Nucl. Sci. Technol.*, 11, 231 (1974), also *Nucl. Sci. Eng.*, 53, 355 (1974).

Figure 11. Problem 1Ai "No scattering" ($x = z = 5$ cm)

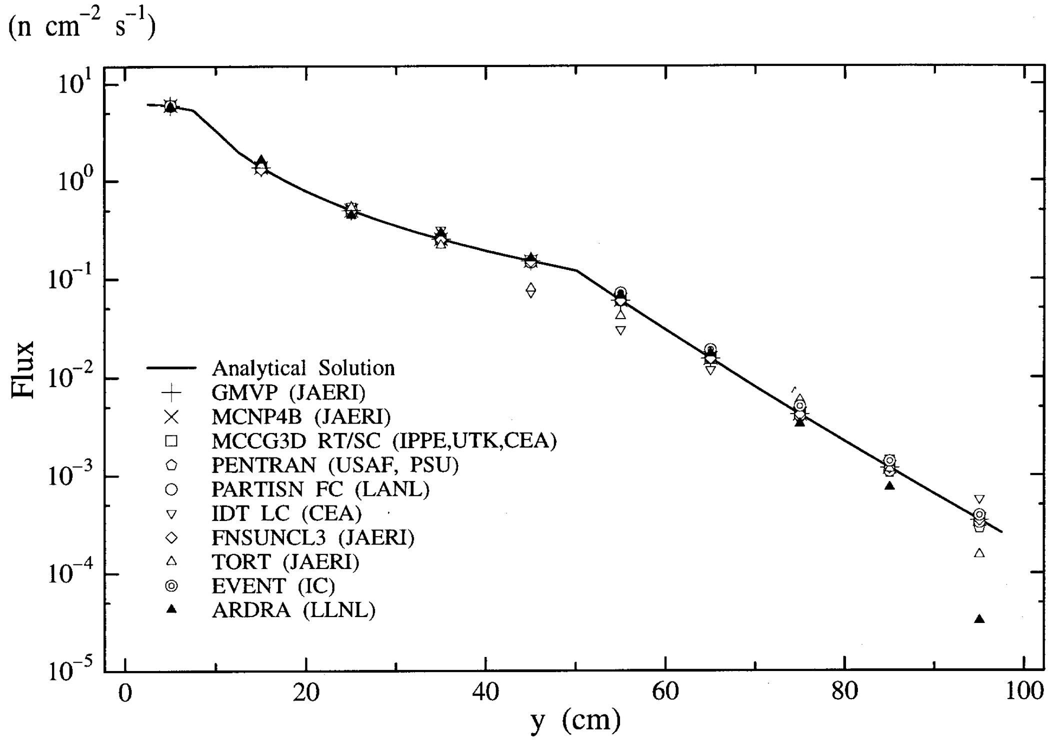

Figure 12. Relative flux of problem 1Ai ($x = z = 5$ cm)

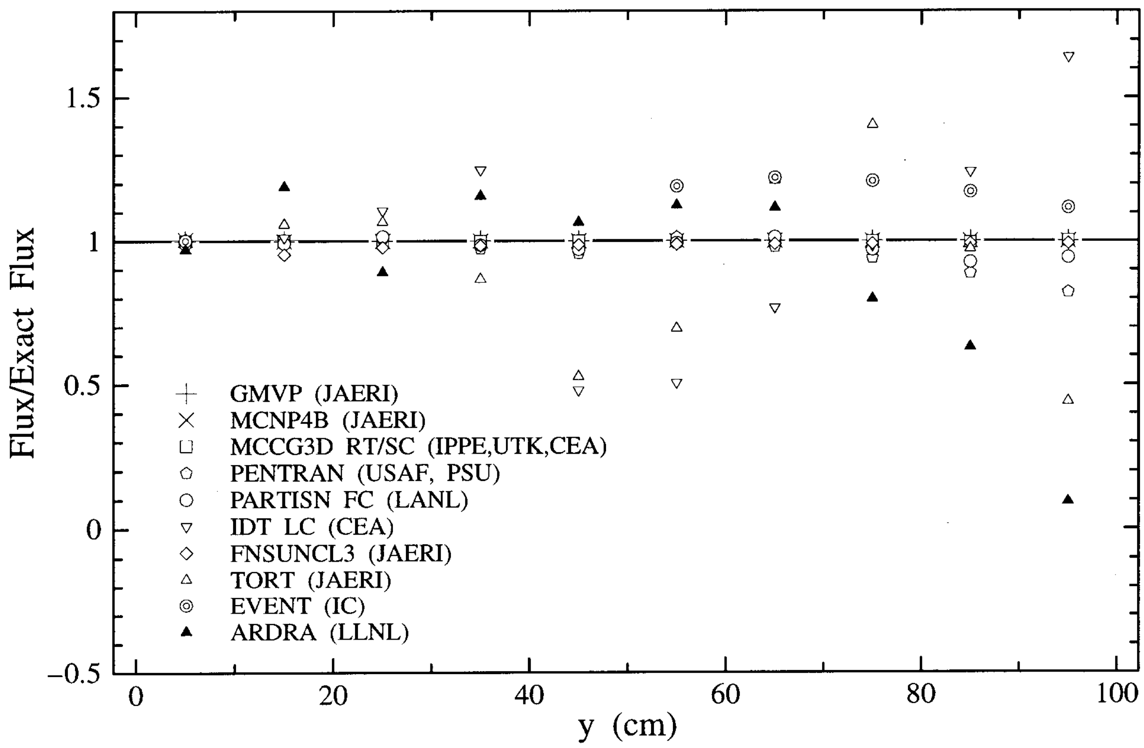

Figure 13. Problem 1Aii "50% scattering" ($x = z = 5$ cm)

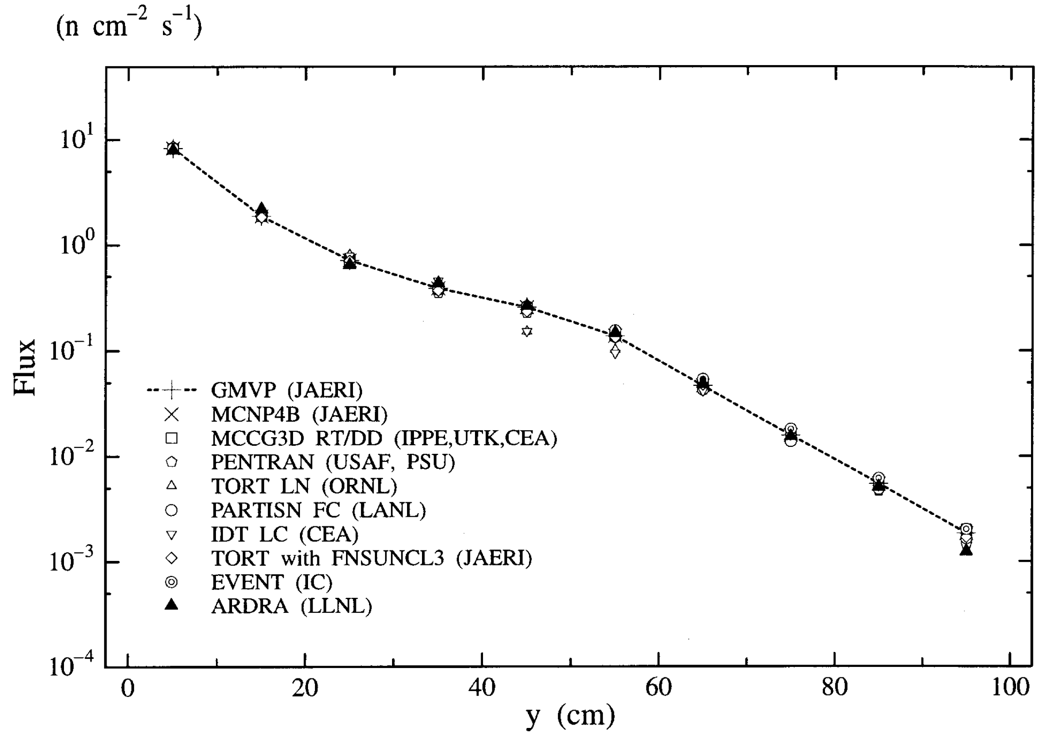

Figure 14. Relative flux of problem 1Aii ($x = z = 5$ cm)

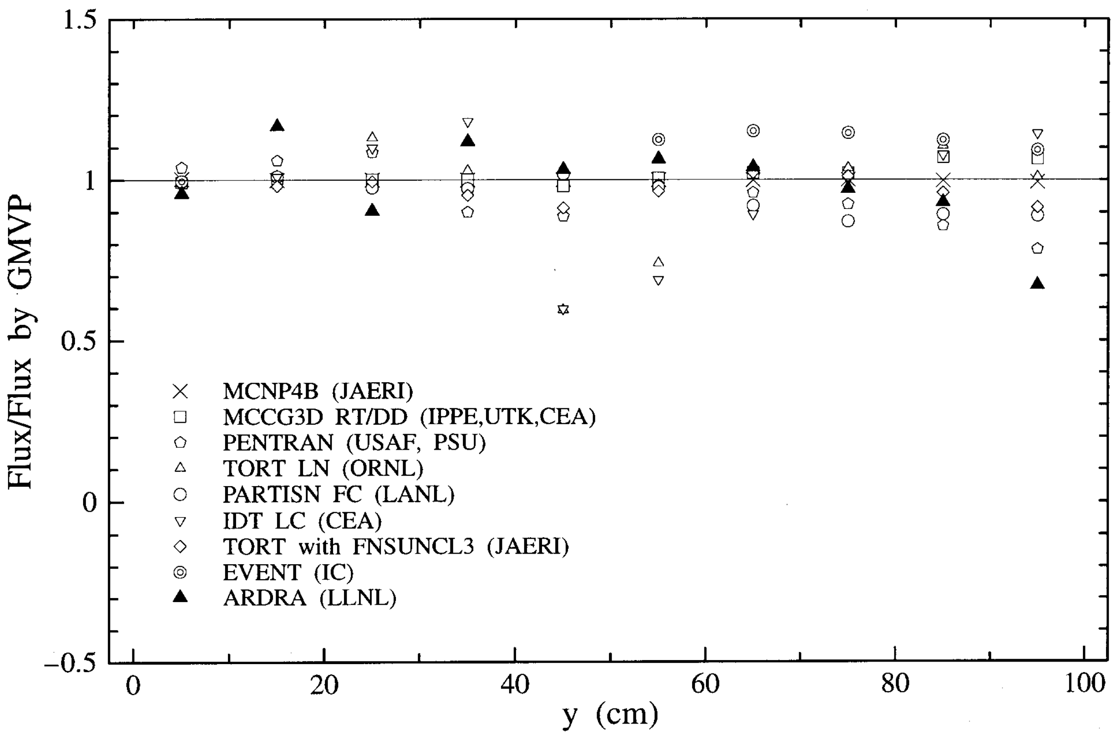

Figure 15. Problem 1Bi "No scattering" ($x = y = z$)

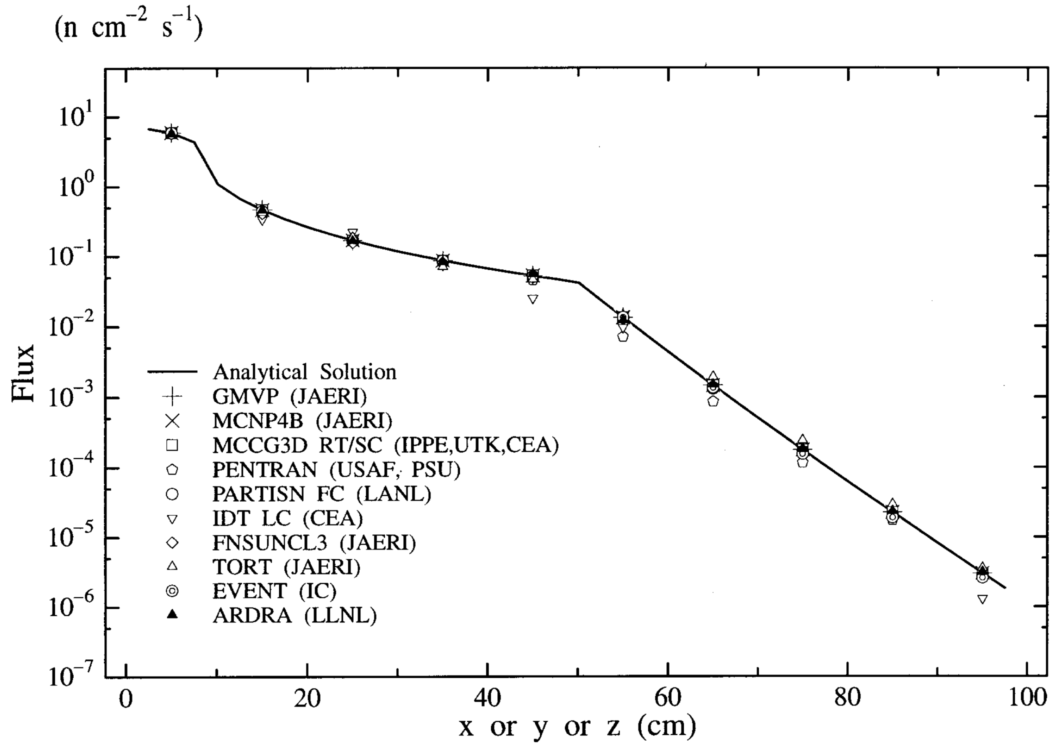

Figure 16. Relative flux of problem 1Bi ($x = y = z$)

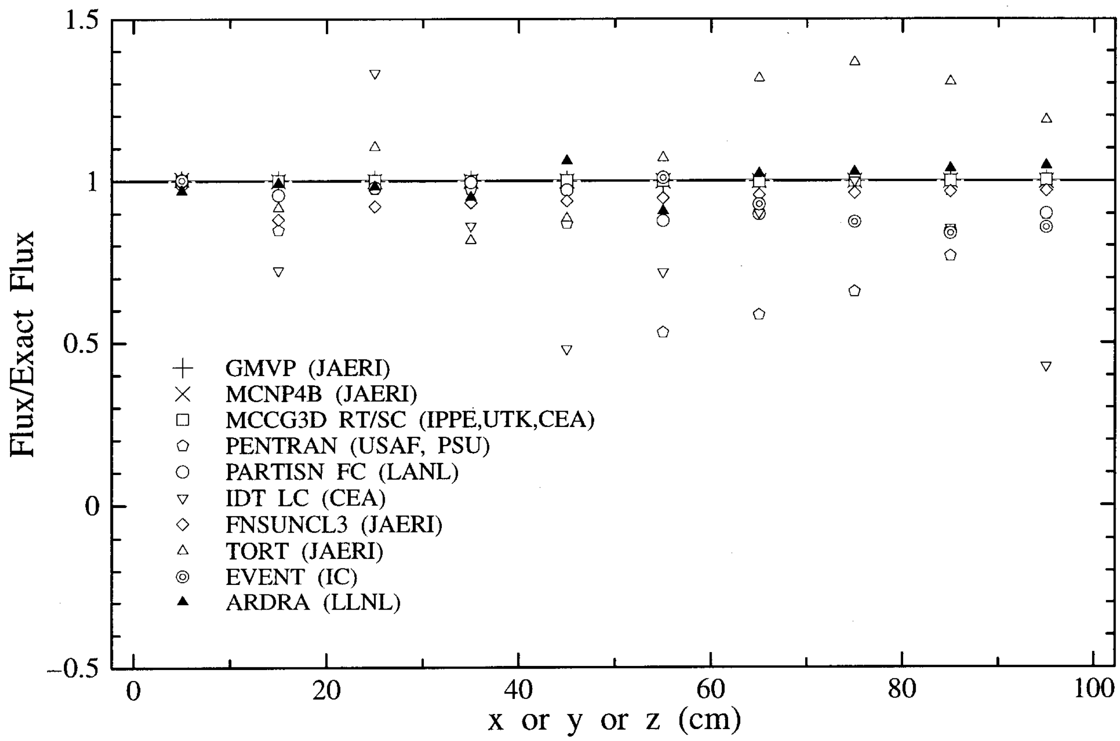

Figure 17. Problem 1Bii “50% scattering” (*x* = *y* = *z*)

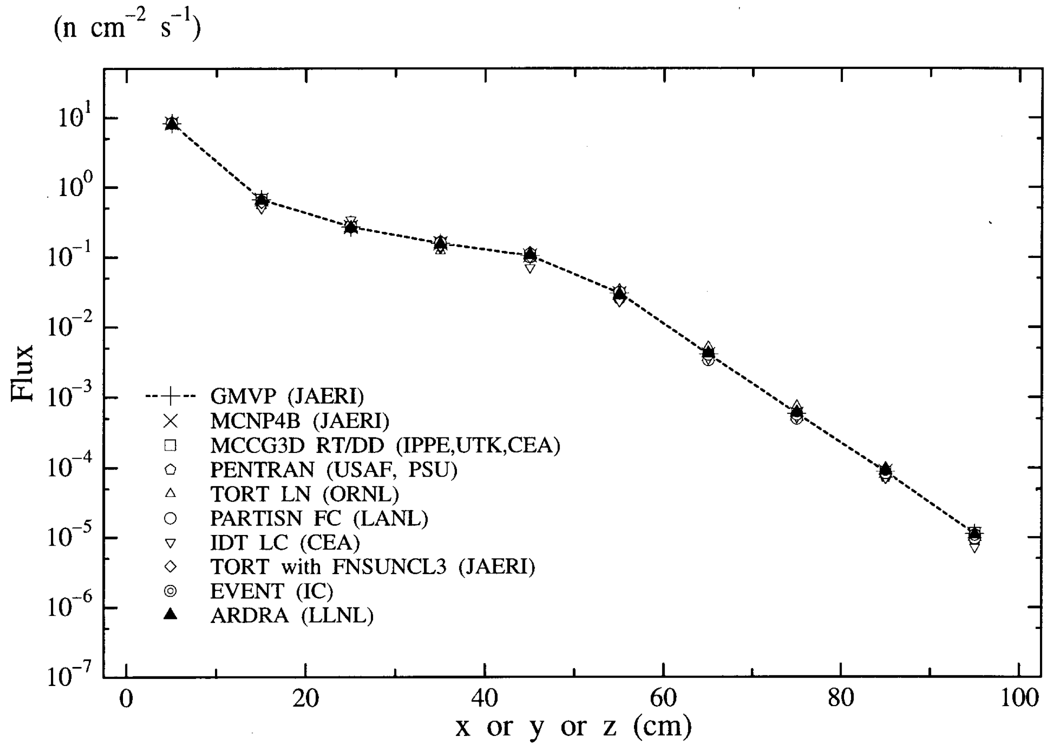

Figure 18. Relative flux of problem 1Bii (*x* = *y* = *z*)

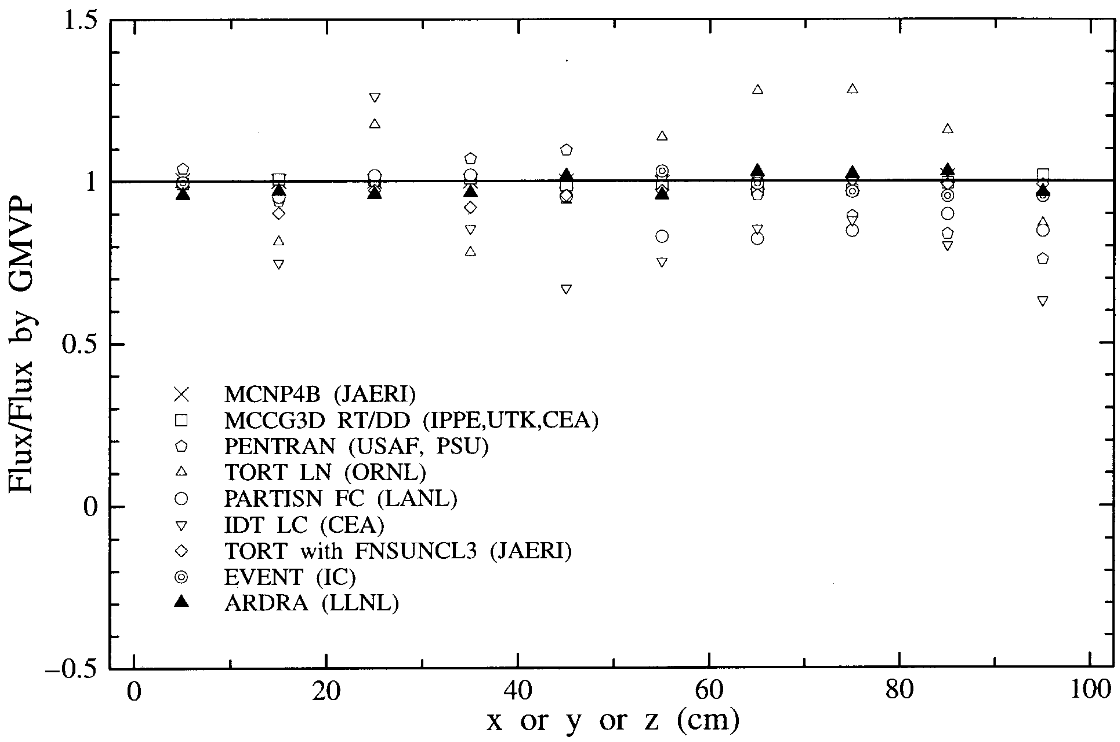

Figure 19. Problem 1Ci "No scattering" (*y* = 55 cm, *z* = 5 cm)

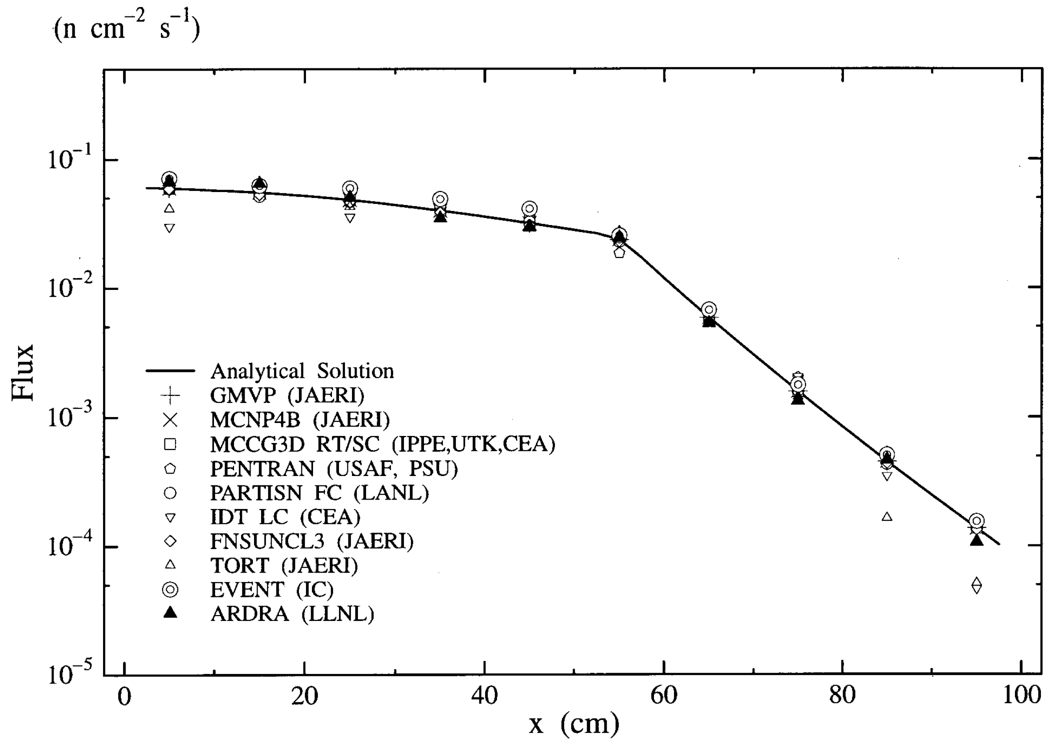

Figure 20. Relative flux of problem 1Ci (*y* = 55 cm, *z* = 5 cm)

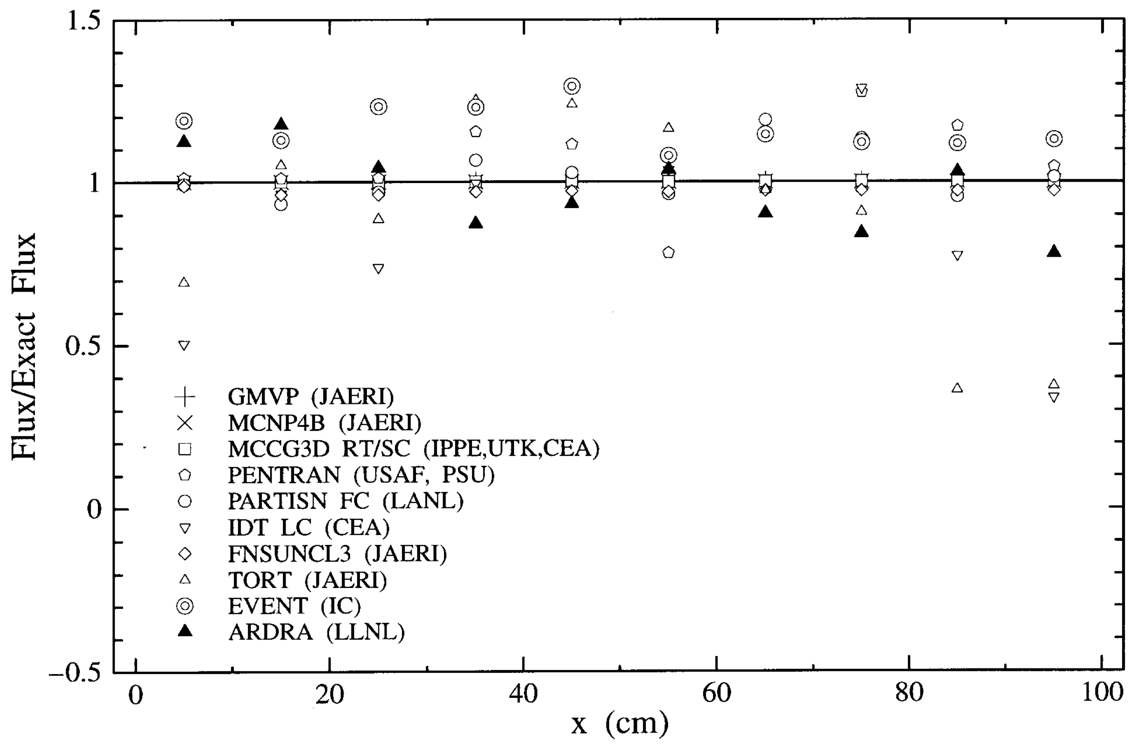

Figure 21. Problem 1Cii "50% scattering" (y = 55 cm, z = 5 cm)

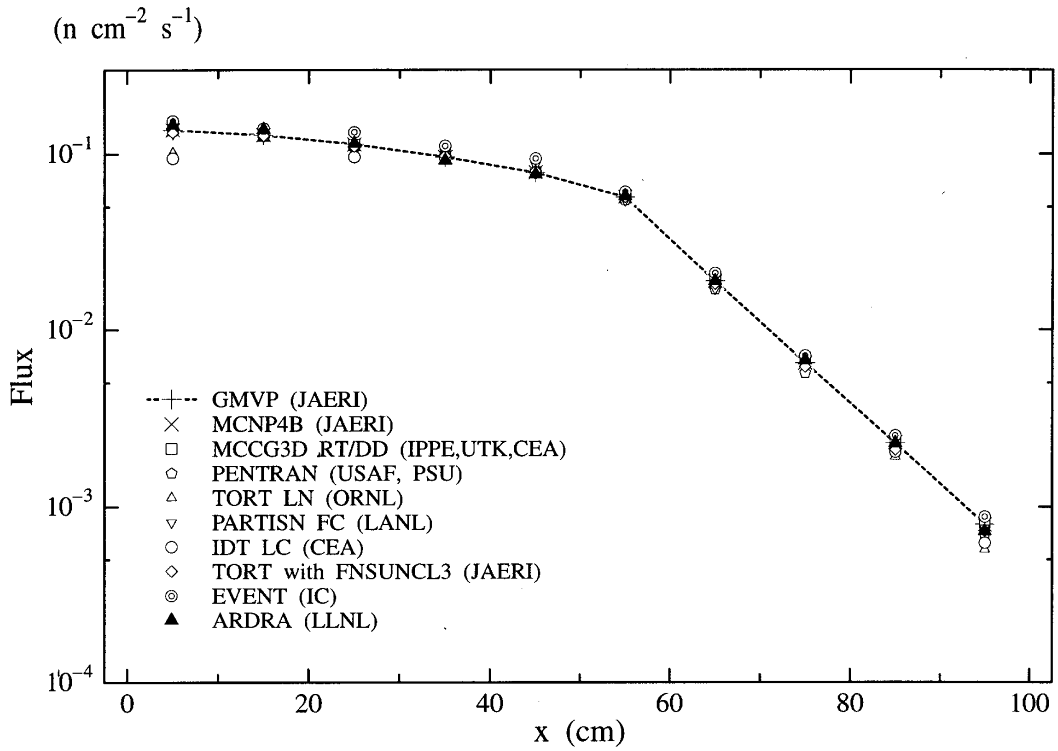

Figure 22. Relative flux of problem 1Cii (y = 55 cm, z = 5 cm)

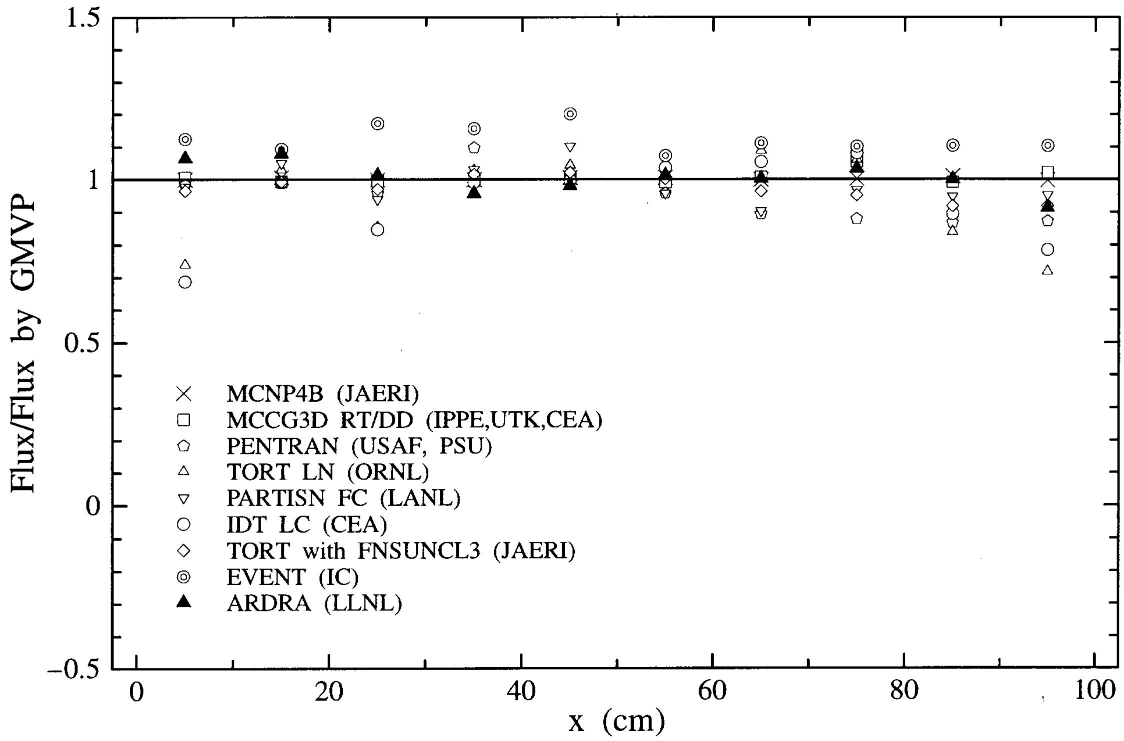

Figure 23. Problem 2Ai "No scattering" (*x* = *z* = 5 cm)

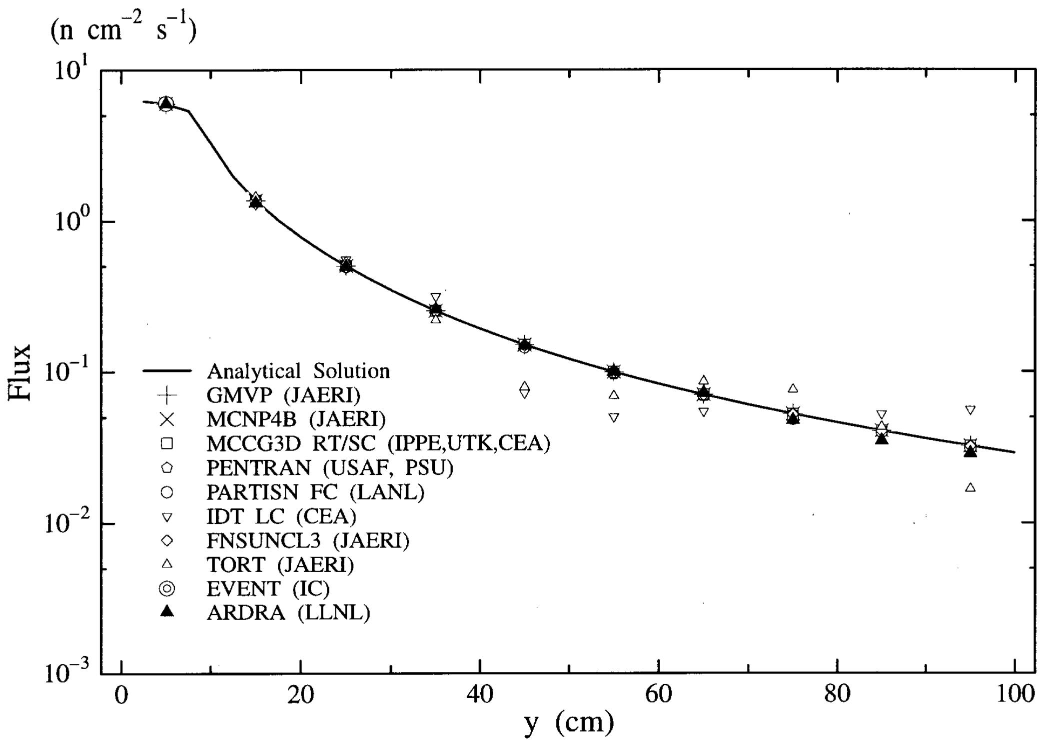

Figure 24. Relative flux of problem 2Ai (*x* = *z* = 5 cm)

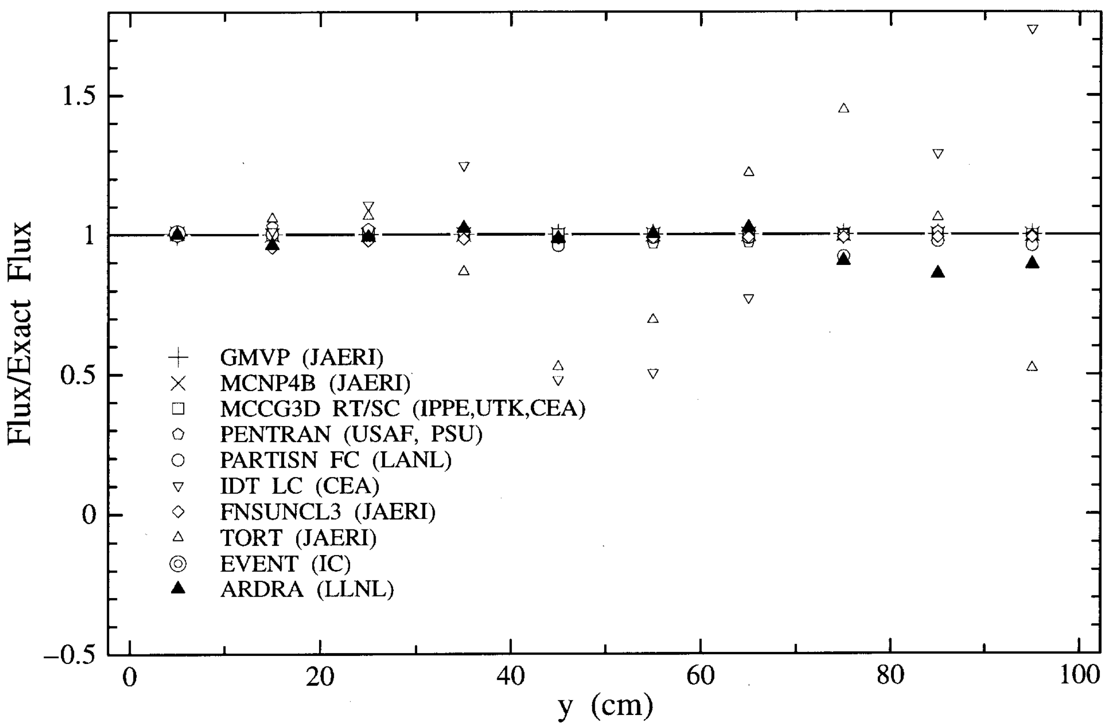

Figure 25. Problem 2Aii "50% scattering" (*x* = *z* = 5 cm)

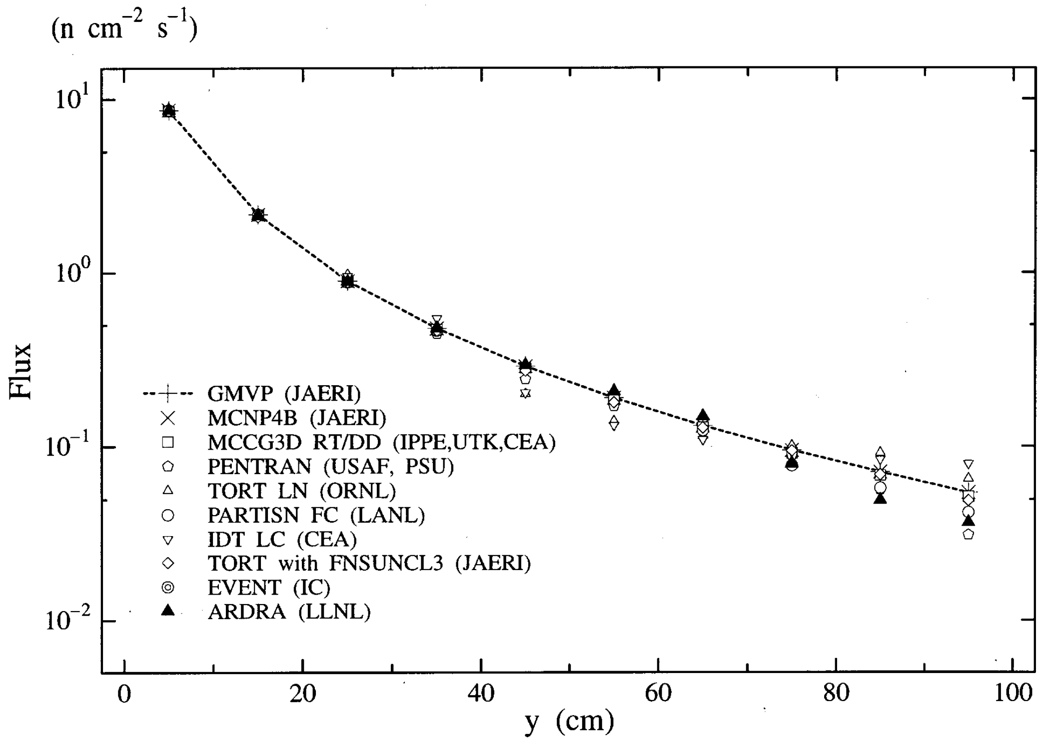

Figure 26. Relative flux of problem 2Aii (*x* = *z* = 5 cm)

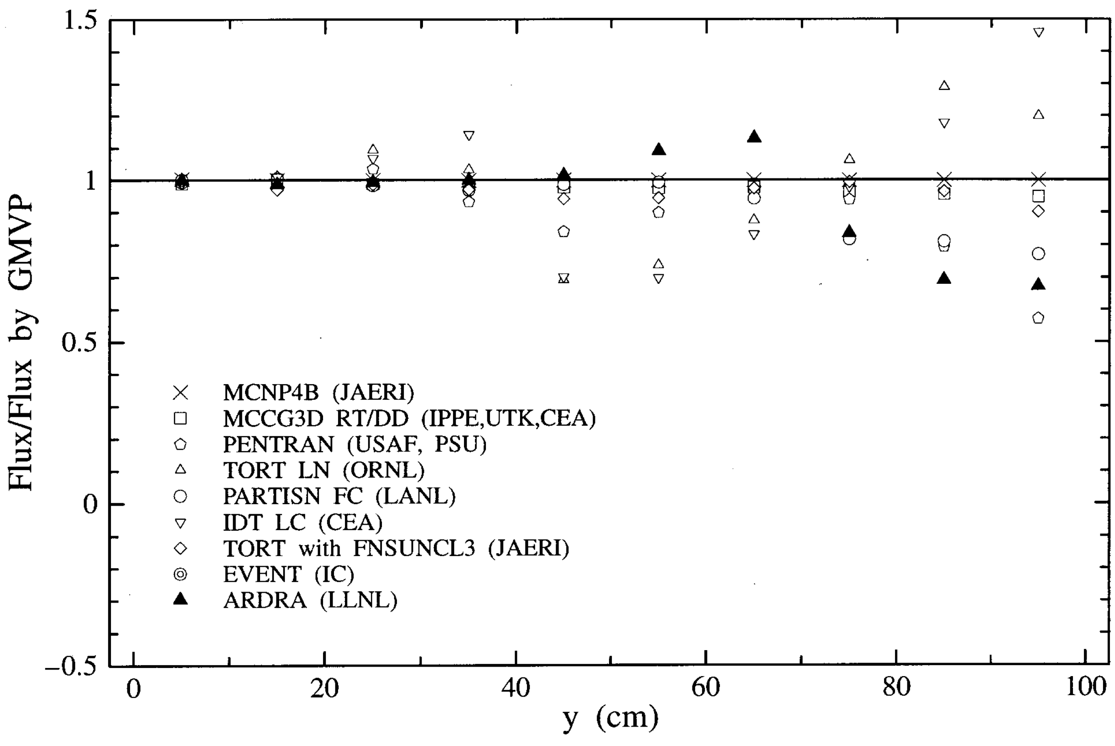

Figure 27. Problem 2Bi "No scattering" (y = 95 cm, z = 5 cm)

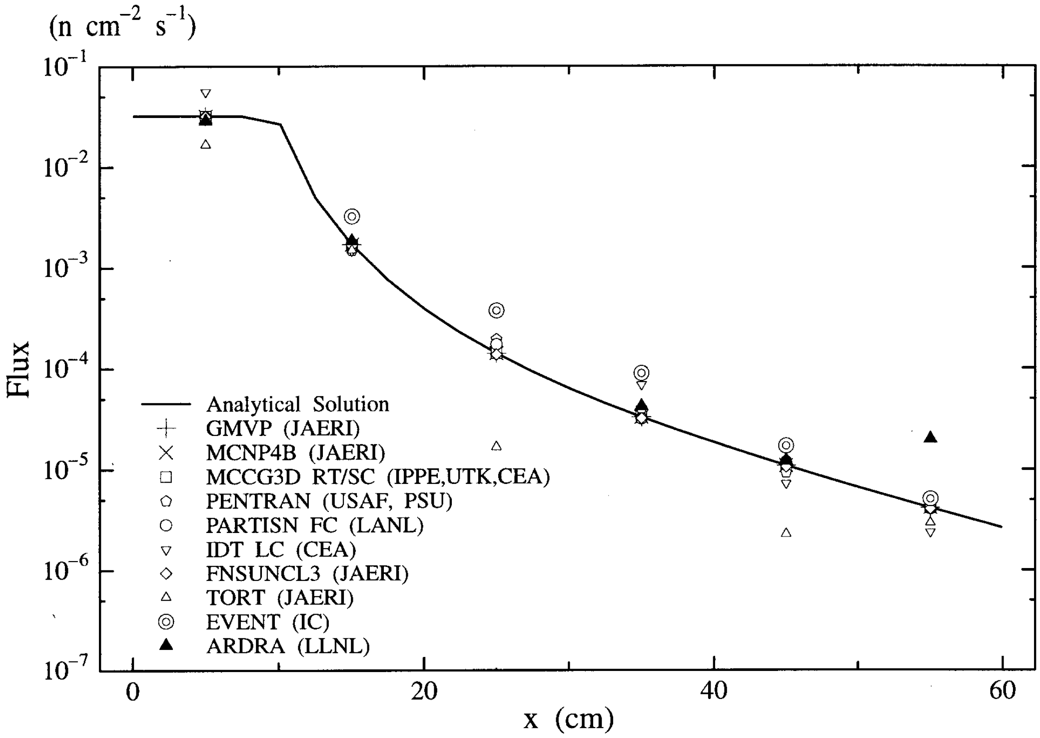

Figure 28. Relative flux of problem 2Bi (y = 95 cm, z = 5 cm)

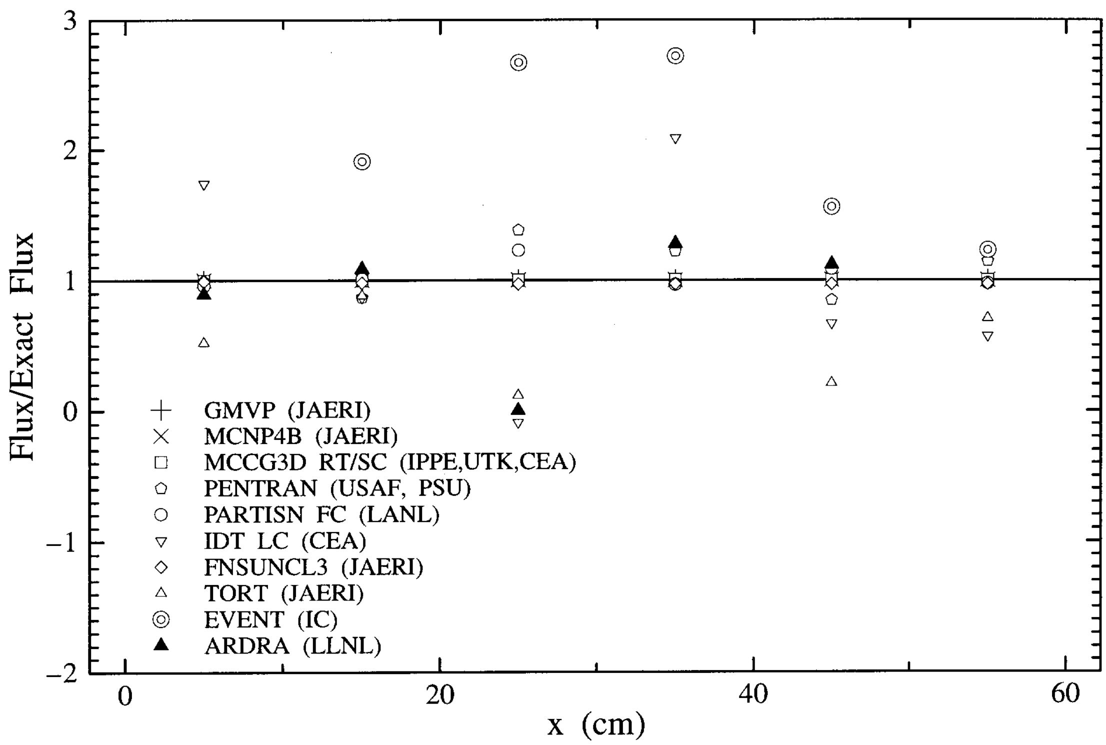

Figure 29. Problem 2Bii "50% scattering" (*y* = 95 cm, *z* = 5 cm)

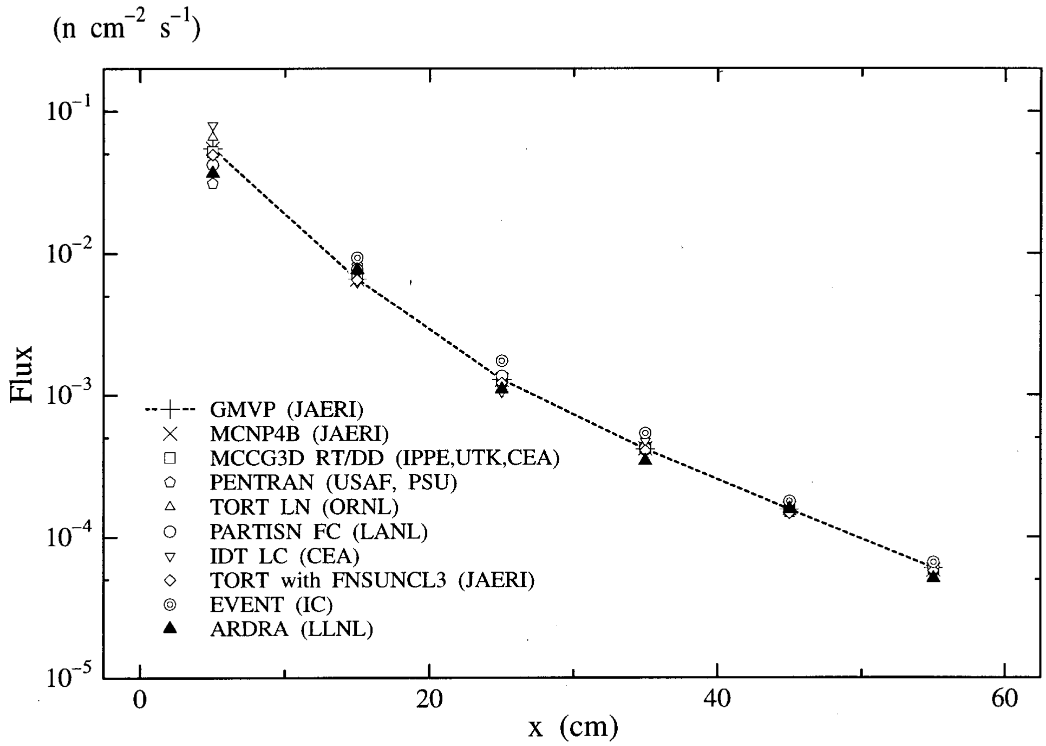

Figure 30. Relative flux of problem 2Bii (*y* = 95 cm, *z* = 5 cm)

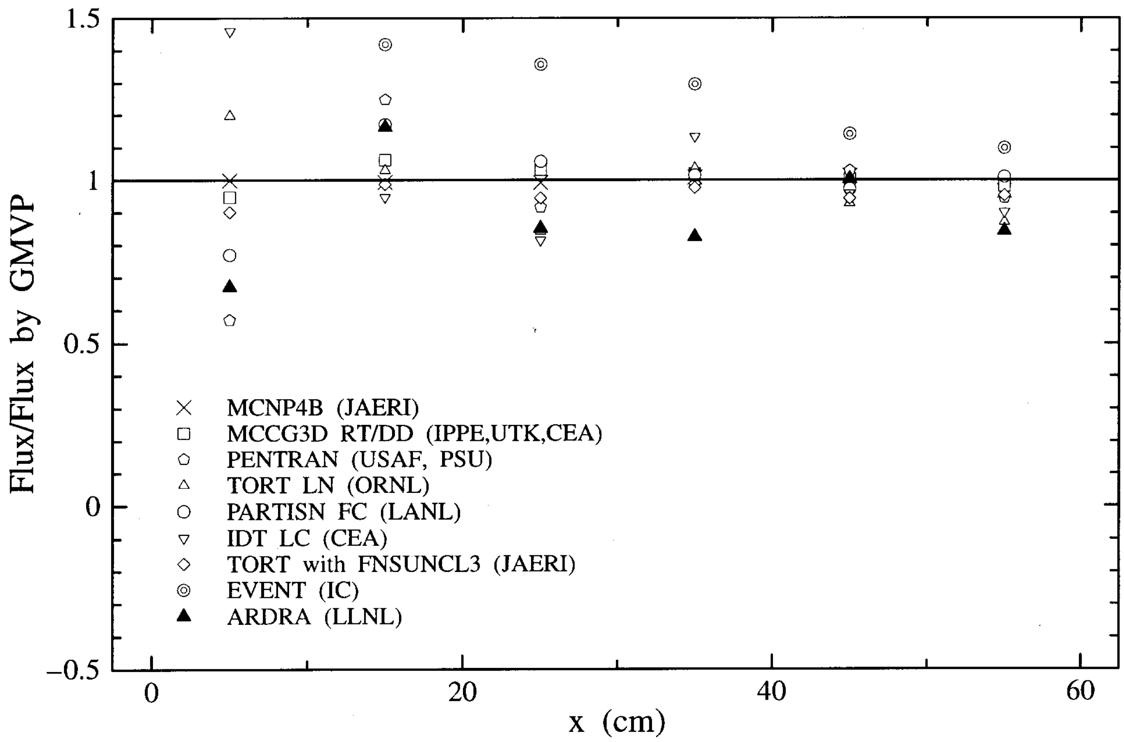

Figure 31. Problem 3Ai "No scattering" (*x* = *z* = 5 cm)

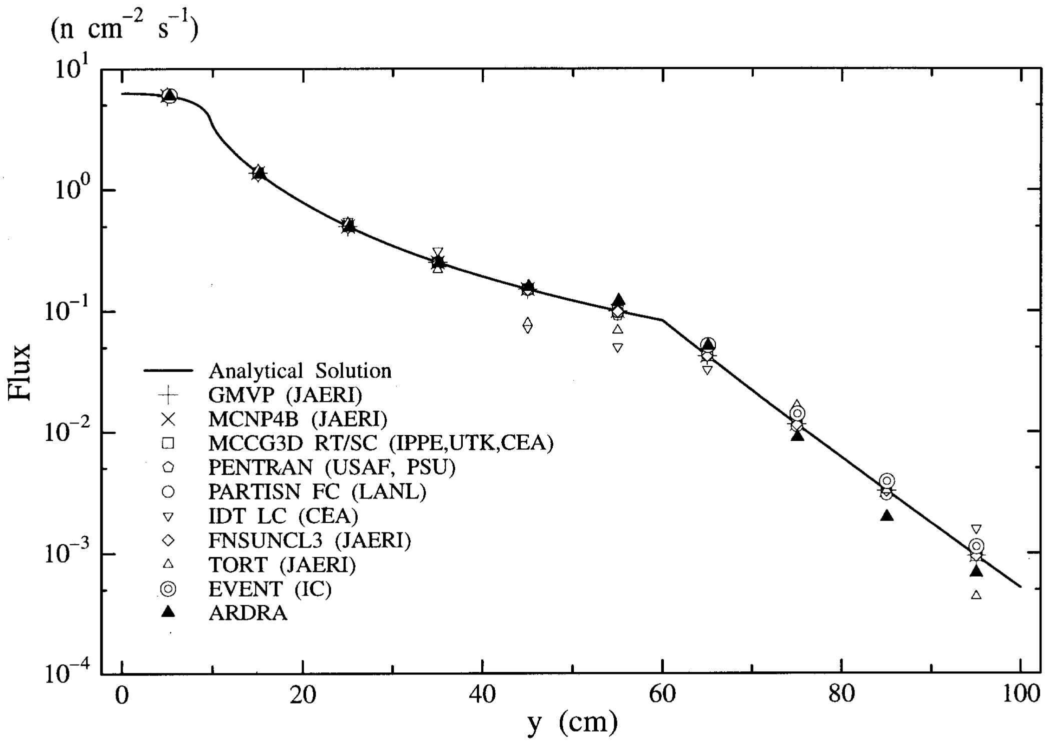

Figure 32. Relative flux of problem 3Ai (*x* = *z* = 5 cm)

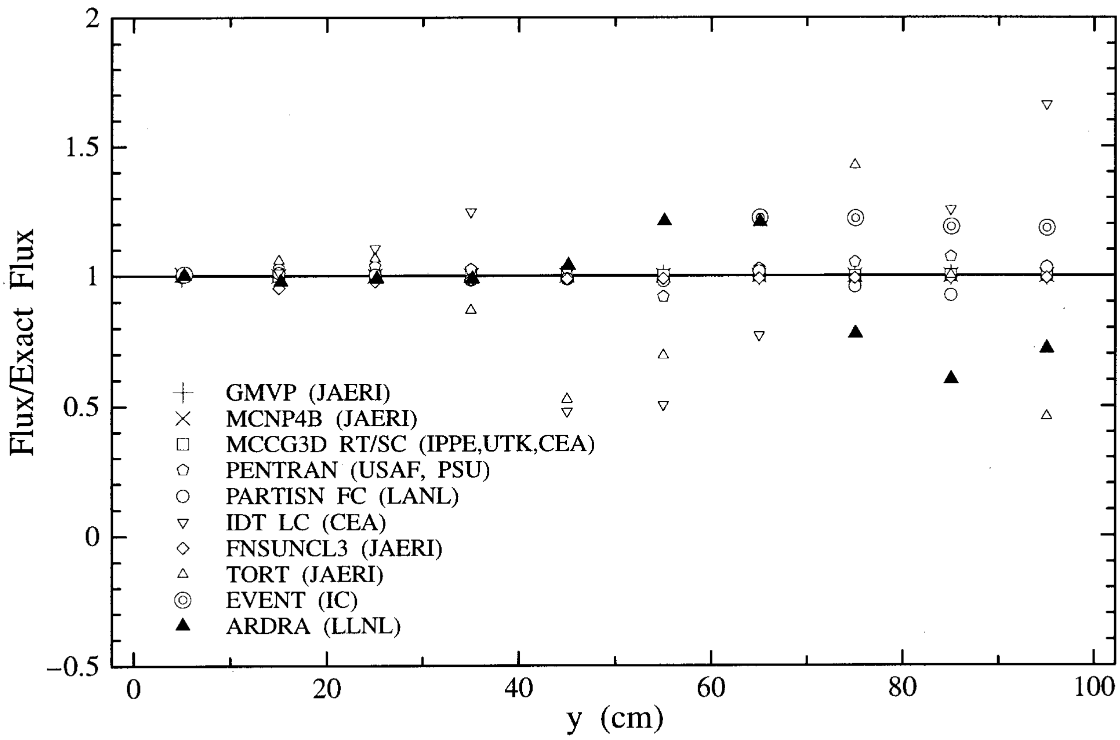

Figure 33. Problem 3Aii "50% scattering" (*x* = *z* = 5 cm)

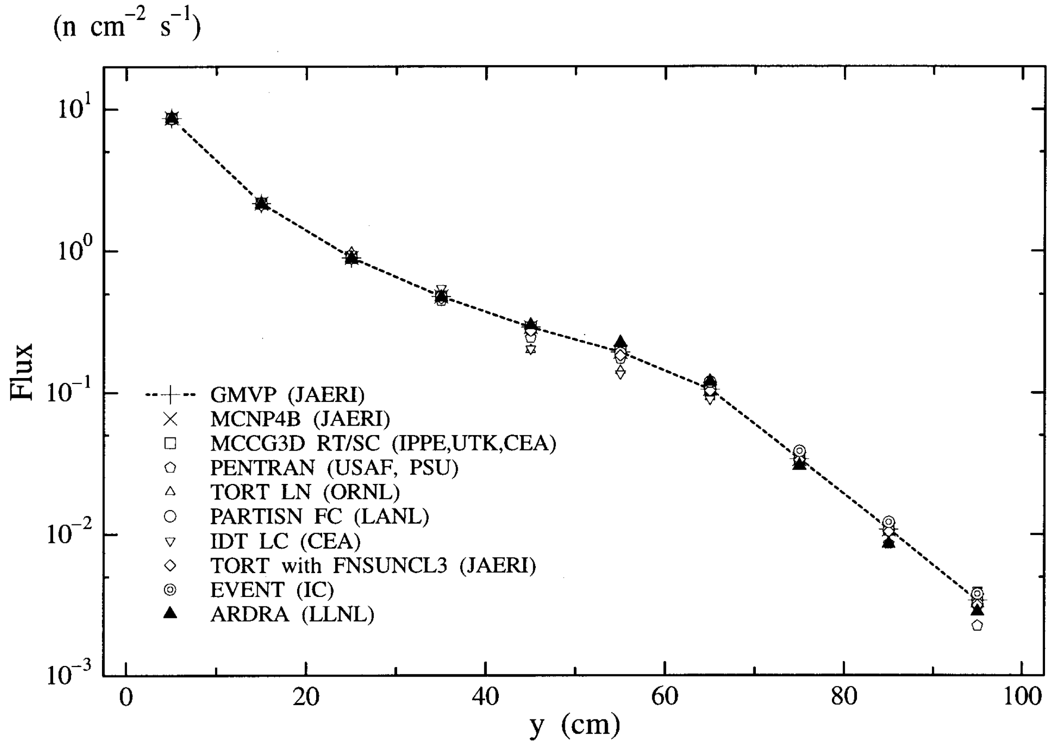

Figure 34. Relative flux of problem 3Aii (*x* = *z* = 5 cm)

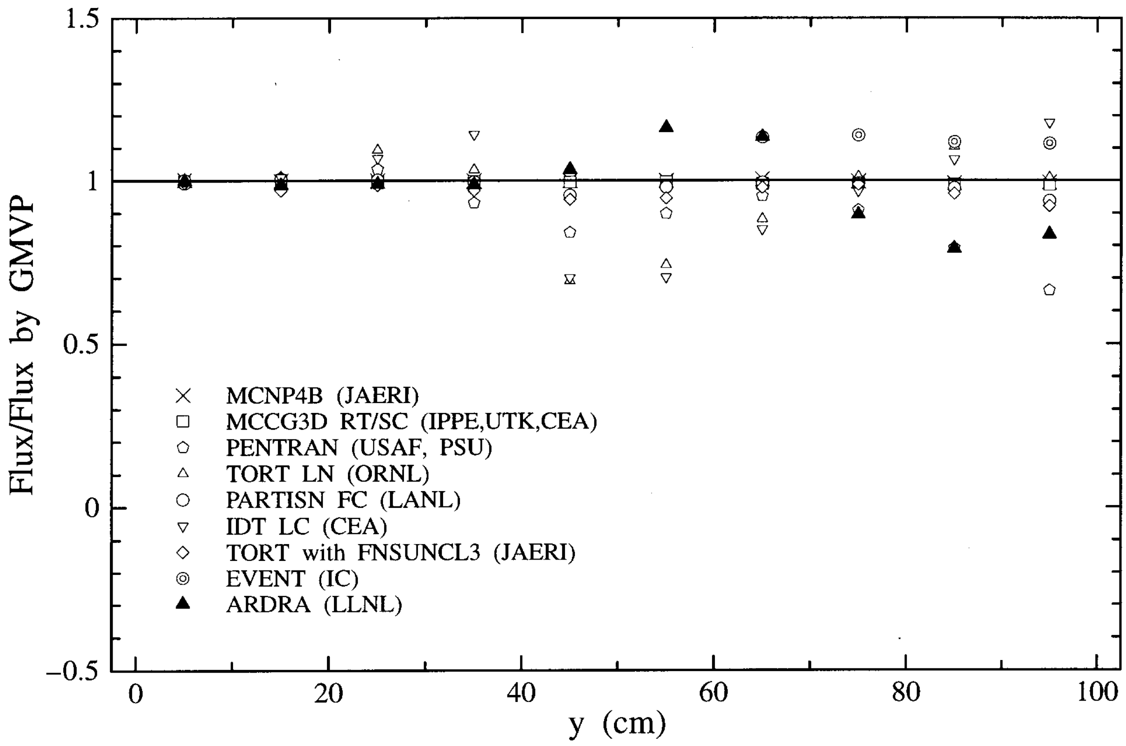

Figure 35. Problem 3Bi "No scattering" (y = 55 cm, z = 5 cm)

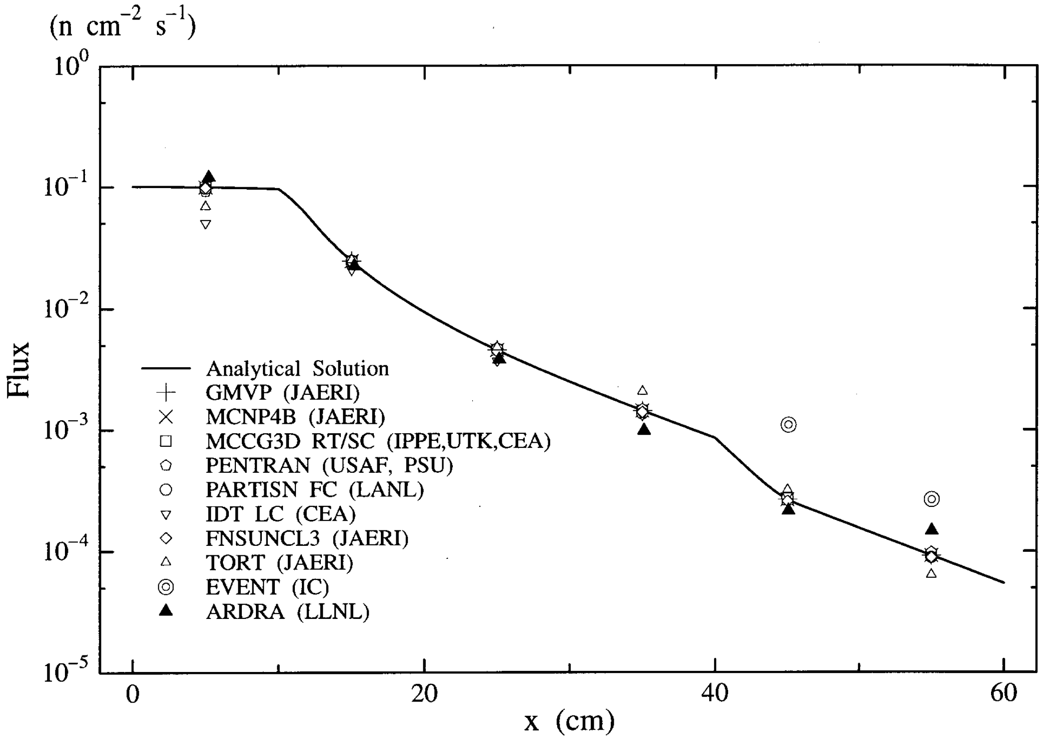

Figure 36. Relative flux of problem 3Bi (y = 55 cm, z = 5 cm)

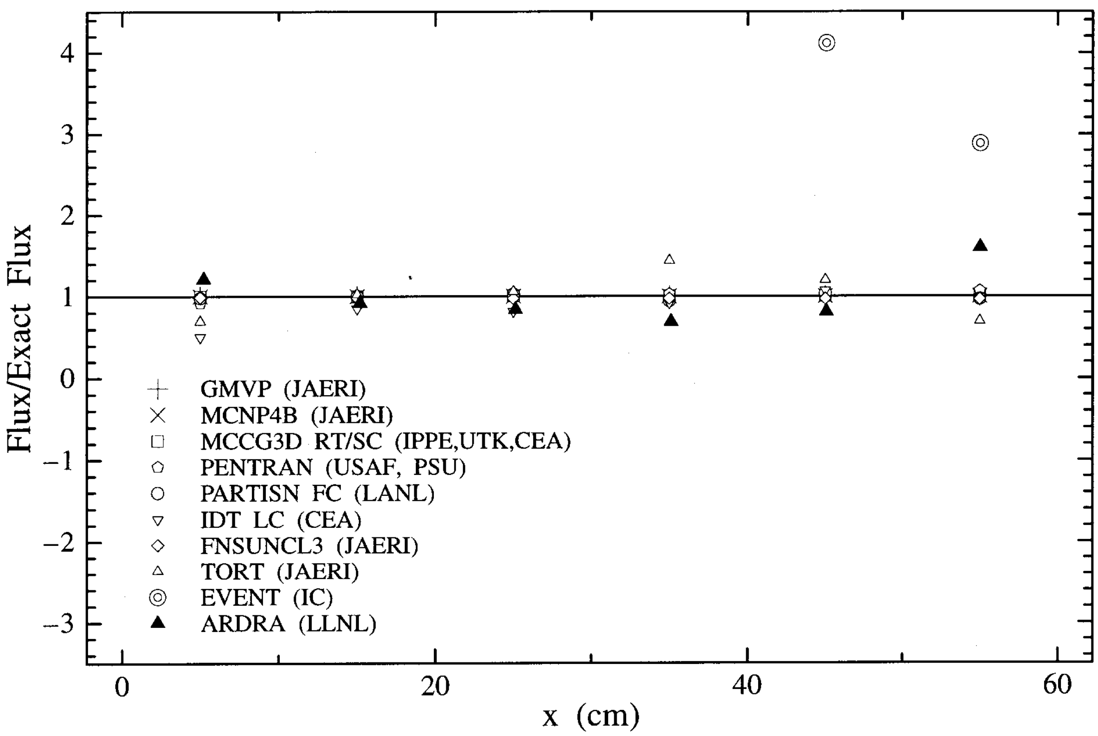

Figure 37. Problem 3Bii "50% scattering" (*y* = 55 cm, *z* = 5 cm)

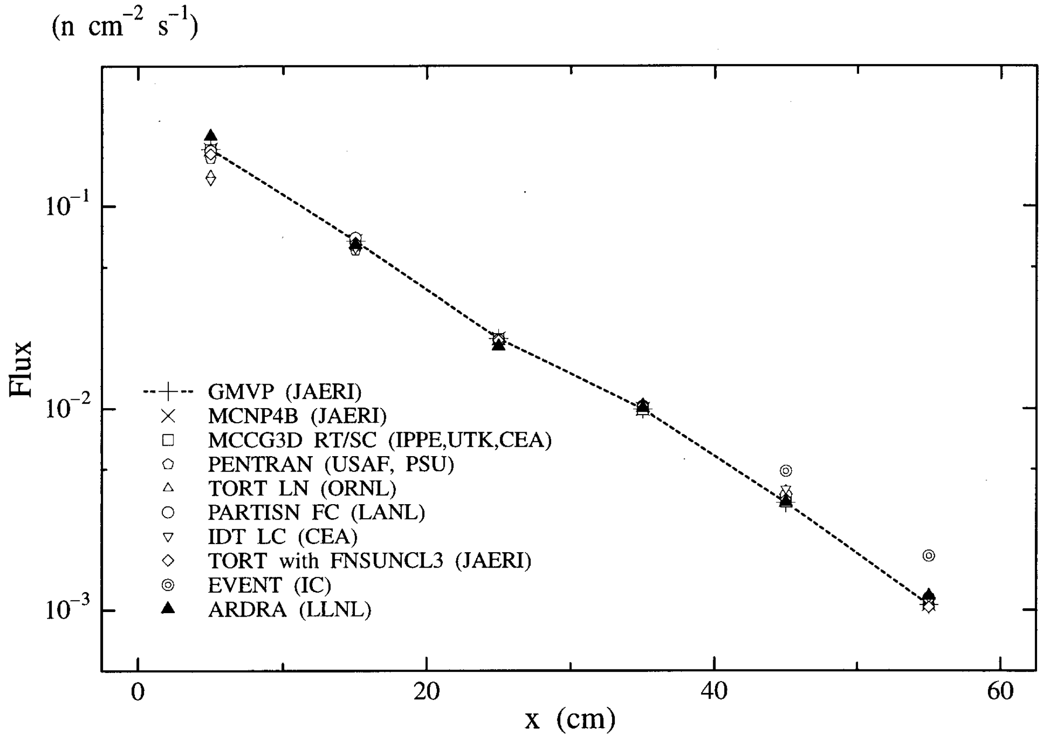

Figure 38. Relative flux of problem 3Bii (*y* = 55 cm, *z* = 5 cm)

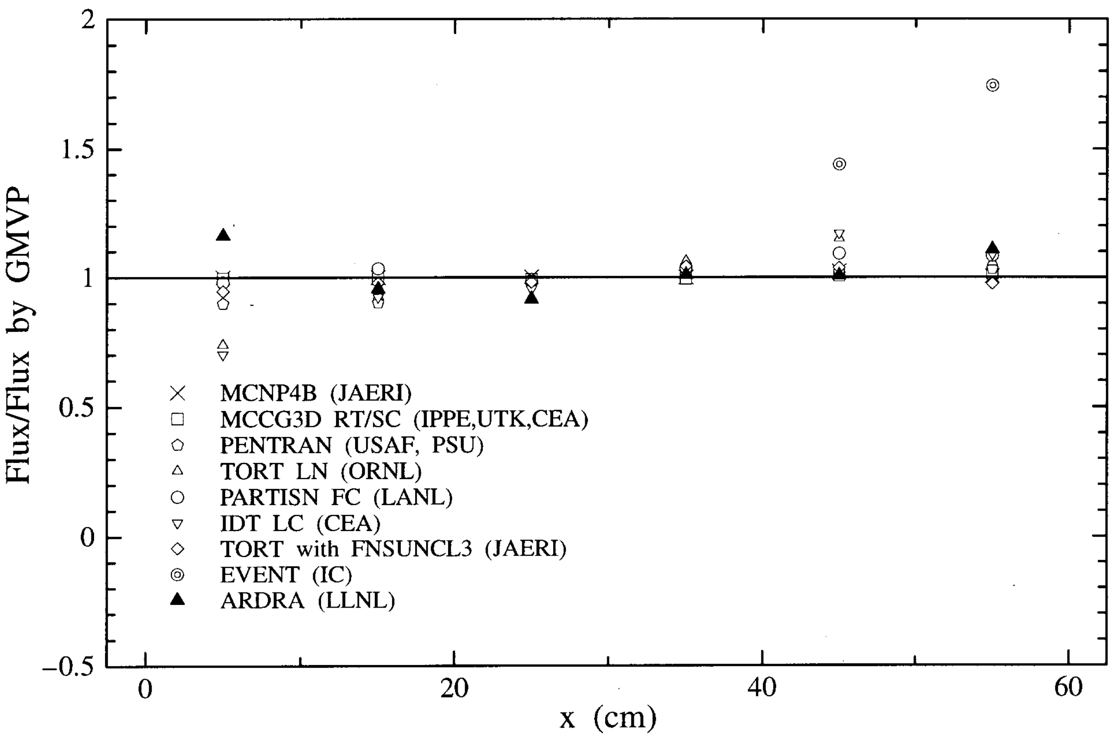

Figure 39. Problem 3Ci "No scattering" (*y* = 95 cm, *z* = 35 cm)

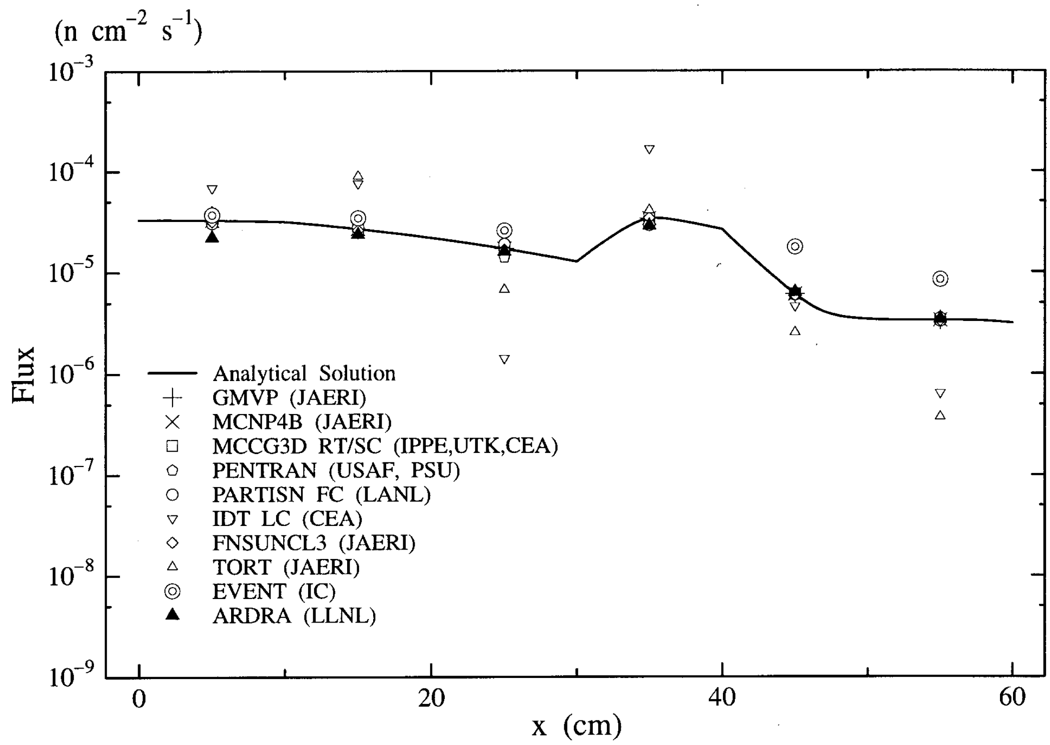

Figure 40. Relative flux of problem 3Ci (*y* = 95 cm, *z* = 35 cm)

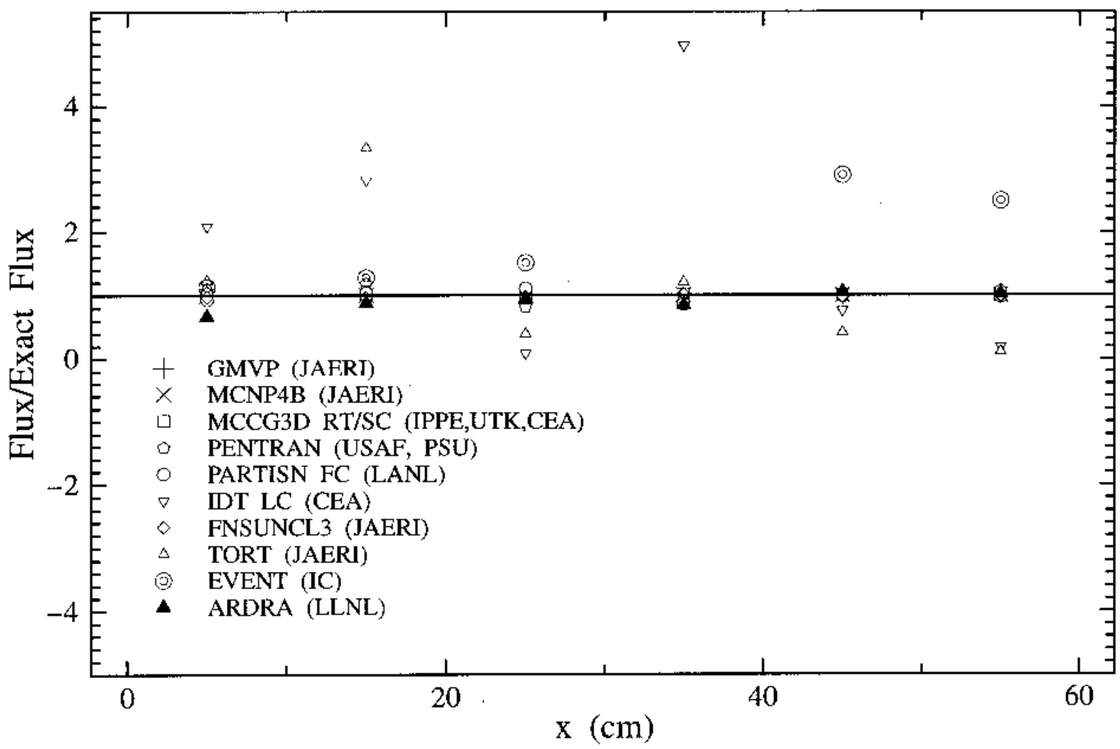

Figure 41. Problem 3Cii "50% scattering" (*y* = 95 cm, *z* = 35 cm)

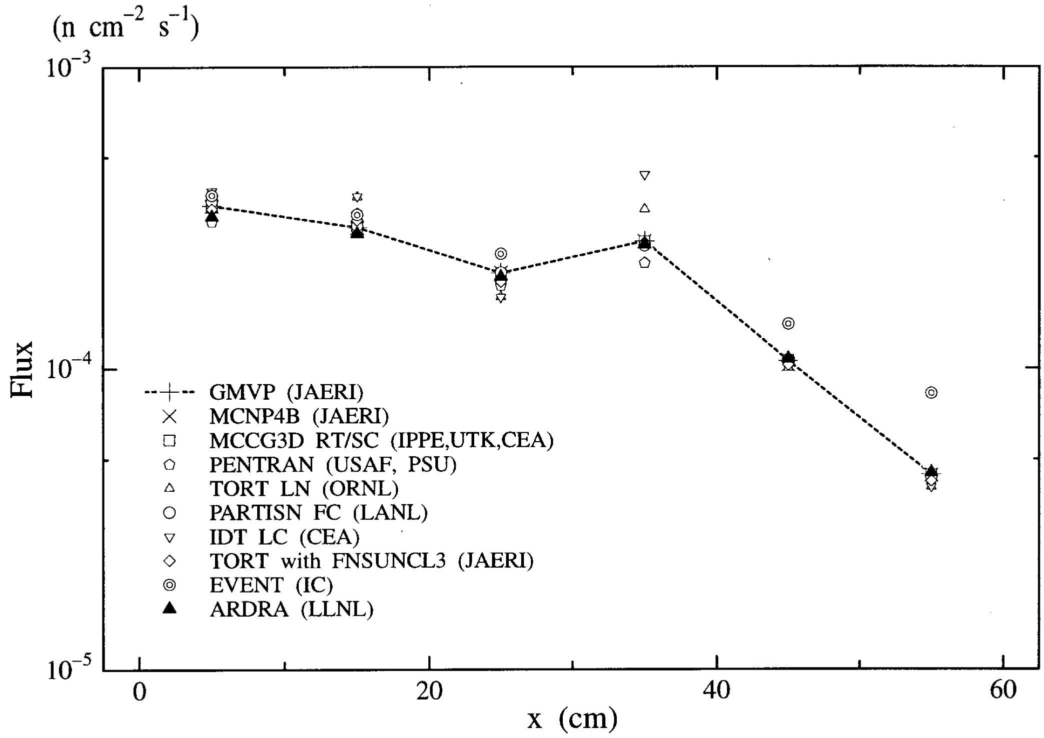

Figure 42. Relative flux of problem 3Cii (*y* = 95 cm, *z* = 35 cm)